Inorganic Molecular Imprinting for Mesoporous NaCl Sensing Material

By

Anum Fiaz

Regn. # 00000117020

A thesis submitted in partial fulfillment of the requirement for the degree
of Master of Science in Chemistry

Supervised by

Dr. Zahida Malik
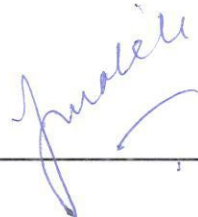
Department of Chemistry

School of Natural Sciences

National University of Sciences & Technology

Islamabad, Pakistan

2018

National University of Sciences & Technology

MS THESIS WORK

We hereby recommend that the dissertation prepared under our supervision by: <u>ANUM FIAZ, Regn No. 00000117020</u> Titled: <u>Inorganic Molecular Imprinting for Mesoporous NaCl Sensing Material</u> be accepted in partial fulfillment of the requirements for the award of **MS** degree.

Examination Committee Members

1. Name: <u>PROF. HABIB NASIR</u> Signature: _____

2. Name: <u>DR. GHULAM MUSTAFA</u> Signature: _____

External Examiner: <u>DR. NASIR MEHBOOB</u> Signature: _____

Supervisor's Name <u>DR. ZAHIDA MALIK</u> Signature: _____

_____
Head of Department

13/08/18
Date

COUNTERSINGED

Date: <u>13/08/8</u>

_____
Dean/Principal

THESIS ACCEPTANCE CERTIFICATE

Certified that final copy of MS thesis written by **Ms. Anum Fiaz**, (Registration No. **00000117020**), of **School of Natural Sciences** has been vetted by undersigned, found complete in all respects as per NUST statutes/regulations, is free of plagiarism, errors, and mistakes and is accepted as partial fulfillment for award of MS/M.Phil degree. It is further certified that necessary amendments as pointed out by GEC members and external examiner of the scholar have also been incorporated in the said thesis.

Signature: _____

Name of Supervisor: Dr. Zahida Malik

Date: _____13/08/18_____

Signature (HoD): _____

Date: _____13/08/18_____

Signature (Dean/Principal): _____

Date: _____13/08/18_____

In the name of Allah, the most Merciful, the Most Kind.

Nothing can happen without ALLAH's will

Dedicated to my father for his continuous efforts in my education, my mother and siblings for their love &prayers

Acknowledgements

Abstract

The present work demonstrates that the unique properties of mesoporous transition metal oxides enable the efficient synthesis of porous NiO, CuO, Fe_2O_3, Co_3O_4 sacrificial templating with NaCl. Mesoporous metal oxides; NiO, CuO, Fe_2O_3, and Co_3O_4, templated by NaCl were synthesized successfully by using an evaporation method, which was the principal development of methodology in this project. The structural characterizations of these porous metal oxides were performed by using XRPD, SEM, AFM and N_2 adsorption techniques. Phase analysis, purity have been confirmed by X-ray powder diffraction (XRPD) which indicated that all the samples are in single phase. Scanning electron microscopy (SEM) elucidated the morphology as cubic NiO, hexagonal CuO, cubic Fe_2O_3 and octahedral Co_3O_4 with average sizes as102, 124, 350 and 275 nm, respectively. AFM study revealed the surface roughness as 89.7, 8.80, 3.52 and 25.5 nm for NiO, CuO, Fe_2O_3, and Co_3O_4, respectively. N_2 adsorption helped in finding the pore size and pore volume along with the type of adsorption isotherm. The as-synthesized templated metal oxides were used as sensors to find the sensitivity and selectivity against the different concentrations of sodium chloride solution. Evidently, the sensor characteristic is linear with excellent correlation (R^2>0.95) within the concentration range 0 to 50 ppm.

Keywords. Molecular Imprinting, Salt Templated, NaCl sensor, BET, Evaporation method.

Table of Contents

References

List of Figures

List of Tables

List of Abbreviations

AFM	Atomic Force Microscopy
BET	Braunauer Emmet Teller
BSE	Back Scattered Electrons
$Co\,(NO_3)_2.6H_2O$	Cobalt nitrate Hexahydrate
Co_3O_4	Cobalt Oxide
CTAB	Hexa cetyl Trimethylammonium Bromide
$Cu\,(NO_3)_2.3H_2O$	Copper Nitrate Trihydrate
CuO	Copper Oxide
DFT	Density Functional Theory
DI	Deionized water
EDS	Energy Dispersive X-ray Detector
ESM	Egg- Shell Membrane
F	Farad
FCC	Face centered Cubic
Fe_2O_3	Iron Oxide
$FeCl_3.6H_2O$	Ferric Chloride Hexahydrate
IDE	Interdigitated Electrode
LCR	Inductance, Capacitance, Resistance
MCM	Mobil Composition of Matter
MRI	Magnetic Resonance Imaging
n	nano
$Ni\,(NO_3)_2.6H_2O$	Nickel Nitrate Hexahydrate
NiO	Nickel Oxide
PMMA	Poly methyl methacrylate
PSPD	Position sensitive Photo diode
PVP	Polyvinyl Pyrrolidone
SBA	Santa Barbara Amorphous
SDBS	Sodium Dodecyl Benzene Sulphonate
SE	Secondary Electrons
TBAB	Tetrabutyl ammonium Bromide
TEM	Transmission Electron Microscopy
XRPD	X-Ray Powder diffraction

Chapter 1

Introduction

Imprinting is an art permitting to render biohomeletic synthesis receipts it creates cavities against a targeted material called the template at a very molecular level. Imprinted metal oxides show discriminatory attachment during the process for the template leading to synthesis of porous product. As mesoporous oxides being used in immense territory of appositeness for instance; drug delivery, chromatography, solid phase extraction, sensors and catalysis etc. [1]. Such porous imprinted inorganic metal oxides can also be the candidates for all such applications.

1.1 Molecular Imprinting and Sensors

Molecular imprinting pertains to particular fundamental interaction betwixt molecules labelled guest along with host, expose a molecular integral [1]. Inorganic molecularly imprinted materials are mechanically and thermally stable and thus have considerable potency. Imprinted materials are eminently selective, particular, or affine as well as in many cases contend with natural receipts due to their specific features. Their synthesis methodology is inexpensive and unequivocal. To achieve excellent selectivity and sensitivity of a sensor towards its analogous analyte is one of the major attempts in biochemical or chemical sensing. The sensitivity may be accomplished in different routes, for instance, in case of mass sensitive transducer by increasing the device frequency. Nonetheless from the material perspective by either growing their accessibility or increasing the number of interaction sites is another viable approach. Out of these two prospects the former turned out to be more doable, because higher amount of template would be required to increase the number of recognition sites, which can inhibit polymerization [2]

1.1.1. Molecular Imprinting Theory. Imprinting is the method of creating tailer made cavities against a targeted material called the template [3]. By means of these cavities, the resulting material have both the physical and chemical identification, capableness, therefore they are also categorized as plastic antibodies or biomimetic receptors [4]. Molecular perception between a receptor (host) and a template (guest) in a matrix desires binding which can be developed only if the irrevocable sites of the guest and host molecules counterpart each other in chemical functionality, size and shape.

Biological systems like antibody antigen, hormone receptor system and enzyme substrate manifest molecular recognition properties that have advanced by natural excerption [5].

1.1.2 Molecular Imprinting Strategies. Bulk and surface imprinting are the two protocols which are occupied to setup sensor layer.

a. Bulk Imprinting. This type of imprinting is generally selected for the molecules with higher masses for example more than a few hundred a.m.u for instance, environmental contaminants, volatile organics, pharmaceutically active compounds, polycyclic aromatic hydrocarbons and others. During this process, the specific template is precisely combined to the precursor. Accordingly the binding spots are located on both; at the exterior of particular sensing material and within the whole bulk of matrix, so it is named as '*Bulk Imprinting*'. The particular sensitive layer in bulk imprinting may entertain nearly enormous number of binding sites, alike superiority of it can be attainable by means of diffusion pathways [2] as shown in figure 1.1.
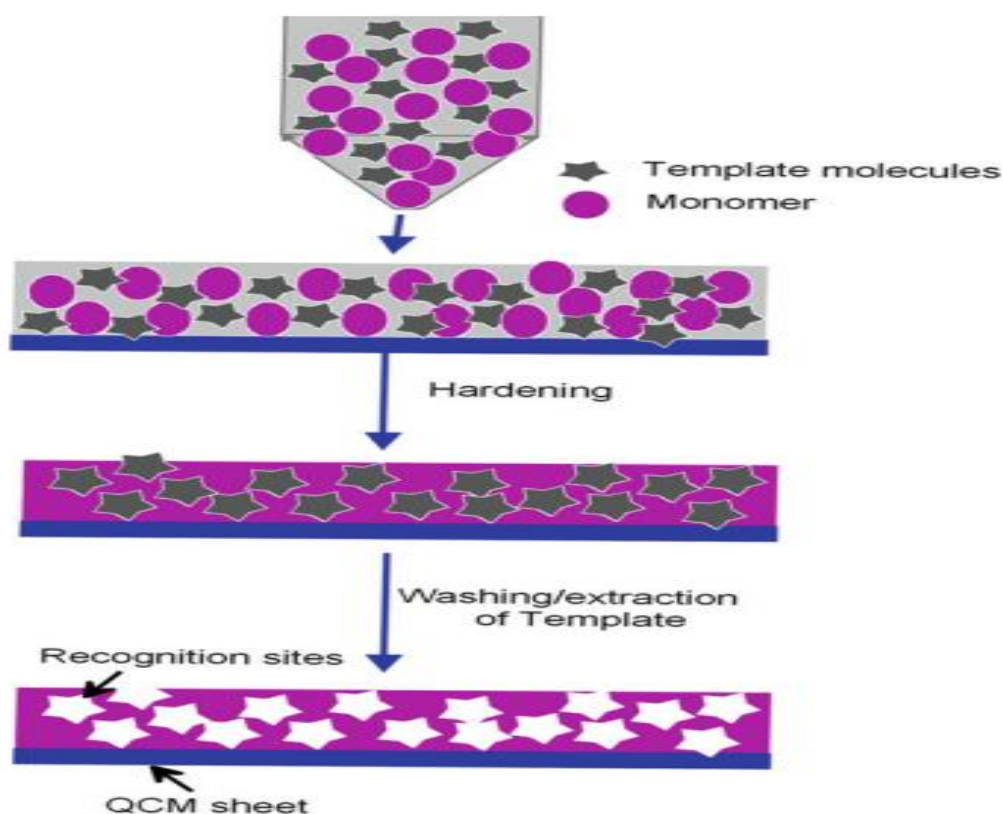
1.1 Bulk imprinting illustration [2]

b. Surface Imprinting. It falls to setup relevant recognition sites, when designing at large size templates for instance. biospecies such as cells and proteins, this is because of the following reasons;

1. The complete removal of template from the matrix is very laborious.
2. The as-obtained materials would be massive and dense for the sensing.
3. Dissemination into the cavities located below the exterior part would be considerably hampered.

To drench the circumstances, surface type of imprinting approach has refined by self-organization of the template species on a mold that is then rushed on to the pre-polymerized material, laminated on to the exterior of the corresponding electrode. This again is persued by drying the material and getting rid of the template. It has cleared that selectivity of these templated materials is dogged by surface chemistry, size along with shape in a same way as for bulk imprinted materials [6]. The general procedure of surface type of imprinting is shown in Figure 1.2.
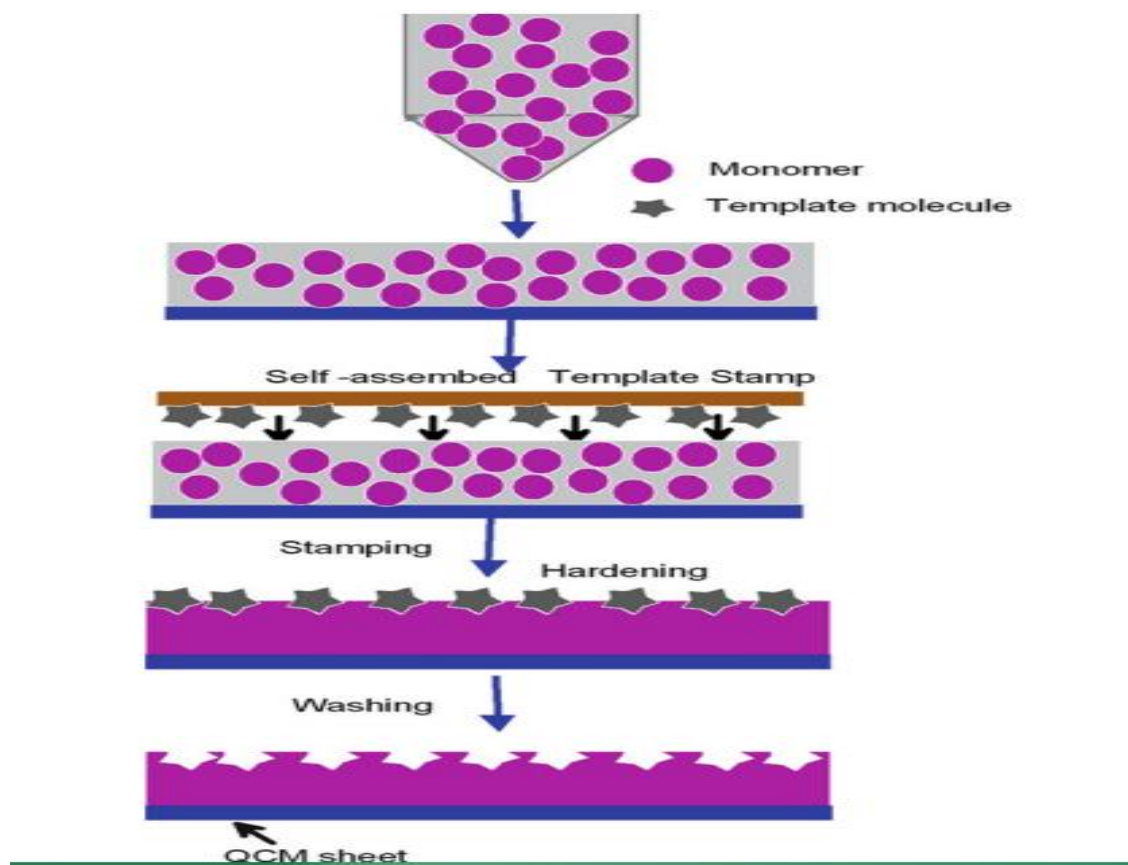
Figure 1.2. surface imprinting illustration [2]

3

c. Imprinted Nanoparticles. Enhanced receptiveness can be executed by administering nanoparticles as a recognized material rather than thin films. Such molecularly imprinted nanoparticles furnish extensively expanded surface for receptor- analyte interaction as correlated to delicate films [7].

1.1.3. Categories of Molecularly Nanoparticles. Positioned on the binding spots or bonds between the analyte and the precursor there are two approaches in molecularly imprinted materials*.*

a.Covalent Based Approach*.* In this approach the template is bonded covalently to metal oxide. In this approach the template is chemically cleaved from the metal oxide. However the necessities of covalent imprinting are distinctive from non-covalent in contemplation of the rate of precursor and the template [8]. Reversible covalent interactions are scanty in number along with frequently need hydrolysis process to break covalent interaction betwixt the metal oxide and template [9].

b .Non-covalent approach. These are based on non-covalent forces like dipole dipole interactions, hydrogen bonding interactions and ion pairing betwixt the template and metal precursor. This is the most frequently used approach to synthesize molecularly imprinted materials due to its simplicity. Washing of template is easier in this approach customarily adepts via continuous extraction [2]. The imprint molecule or template interacts with the metal oxide by non-covalent bond during both; the imprinting and rebinding procedures [5]. Restrictions of non-covalent imprinting are appointed by distinctive or unique recognition circumstances. The development of bonding between the template and metal precursor are sustained beneath hydrophobic situation, although polar surroundings rattled them effortlessly. Non-covalent approach is far accessible or effortless than covalent approach or it also generates greater binding sites [10]. Figure 1.3 describes covalent or non-covalent imprinting procedure schematically.
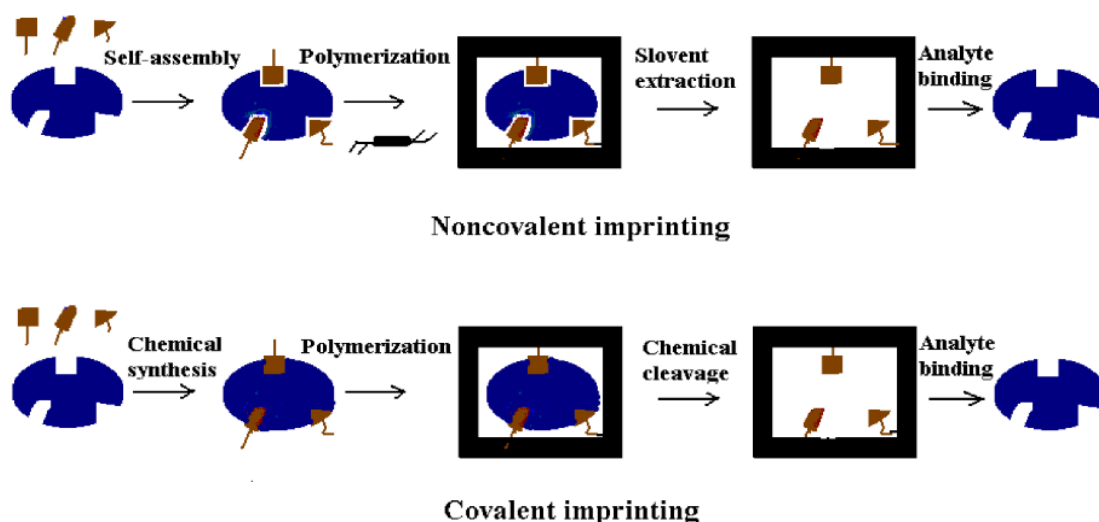
Figure 1.3.covalent or non-covalent imprinting procedure *[8]*

1.1.4. Applications of Molecular Imprinting. There are reports on rewards of molecular imprinted materials, including; higher affinity for target molecule, low cost, higher strength, durability and physical robustness, stability, higher selectivity, long storage life, inertness towards bases, acids, organic solvents and metal ions [7], etc. Few reported applications of molecular imprinting are biological antibodies [11], drug delivery [12], catalysis [13], separation science or purification [4] and chemical sensors [14].

1.2 Molecularly Imprinted Sensors. Molecularly imprinted materials are specifically advisable for the perception in sensing, by virtue of their incorporative immense selectivity having comparatively low-price. Encompassed by else, this undergoes to steadily booming publications in the field. Roughly estimating, sensors are abridged appliances competent of frequently observing chemical components accessible to gases , liquids along with transforming the information into an optical and electrical signal [2]. Biosensors and chemical sensors have expanding interest within the area of contemporary chemistry, at the time that can be recognized from both the divergence of approaches and techniques practiced and from of papers published. It is necessarily due to novel opportunities and appeals that are emerging principally in clinical ailments, food inquiries, environmental scrutiny, manufacture auditing, along with the detection of furtive drugs and chemical warfare agents [15].

1.2.1 Sensing of Cl^-. Sensing of this ion is imperative in many areas such as industrial applications, clinical ailments and climate auditing.

a. Sea water. Sea water is approximately an adequately robust solution of diverse salts. The salt quantity for instance amount of inorganic material in solution, nominated just

5

as salinity or asserted in Kg, g or ppt having Ca^{+2}, Na^{+1}, K^{+1}, Mg^{+2} as prevalent cations, or hydrogen carbonate, sulfate, chloride and bromide as prevalent anions. As the chemical composition of sea water remains quietly perpetual, just one measurement is sufficient to resolve the salt quantity. Thus salinity is confirmed via checking the chloride amount because it is the rich anion in marine water [16].

b. Medical. Chloride ion is a fundamental constituent of the body fluids for adjusting volume of cell, pH along with reticence of human myeloperoxidase. Greater amount of Cl^{-1} is detrimental for both fish and all other marine life [12]. Cl^{-1} plays an important role in anatomical processes. It is not astonishing that unchecked Cl^{-1} can cause deliberate problems [17]. In cystic fibrosis a gene encrypting of a protein, called cystic fibrosis transmembrane regulator , or in epithelial membrane which functions as a Cl^{-1} channel, become mutated and so its objective is transformed. Thus monitoring of Cl^{-1} is not only important in patients, but monitoring in the surrounding is also desired [18].

c. Sweat Analysis. Human sweat contains various ions such as Cl^-, K^+ and Na^+, etc. The composition of sweat differs with human physiological circumstances, which hooks up to drug abuse, therapeutic defects, meal and nutritive salt consumption and parchedness beneath different circumstances. The concentrations of Cl^- and Na^+ ions in sweat give clue of dehydration. consequently cognition of sweat content is an auspicious path to approach human anatomical condition like salt loss and hydration condition [19].

d. Cell Electrolyte Transport. Cl^{-1} ion is crucial electrolyte included in air way fluid balance, blood pressure maintenance, cell volume control, and neuron excitability nociception along with transcellular electrolyte transport. Chloride is merely or specifically monitored in distinct types of cell; it is controlled at moderate (30.5-60.5 mM) concentration in cells, and plunges at a very low (10.5mM) in actively transporting neuron or epithelia. Misregulation of Cl^{-1} ion is correlated with diseases, like epilepsy along with hypertension. Low Cl^{-1} ion engenders cell cycle arrest and Cl^{-1} ion concentration may alter thoroughly as an objective of osmotic stress [20].

e. Marine life. The amount of salt present in sea or rivers is termed as salinity. Each element has a convinced outcome on the breath assisting under a roof of sea water. Salinity is revealed through electrical conductivity in accordance with a unit distance

at a distinct degrees. Many causes effect the level of salinity in the water bodies for instance climate changes, rise in temperature, discharging of water material and oil spills in sea. The consequences of the increment of the salt concentration in sea are destructive for plant species [21]. That is why there should be efficient sensing setup for salinity monitoring in marine environment.

f. Plant growth. The seed germination and growth of plants is distressed by minor modification in salt content. Small increment in salinity raise the density of river so dropping it to the ground and drifting across the river basis. Higher level of salinity can leaven obstacle in deriving water from the soil. This may be noxious to seedling [21].

g. Concrete. Quality of reinforced concrete is determined by its chloride ion contents. These ions initiate the corrosion process and convince depassivation of steel bars, thus leading to a deterioration of a structure. Cl^{-1} ion in concrete appear from water utilized for constituting concrete, from cement, by dissipation of Cl^{-1} ion from exterior of the structure via water pores in concrete and by aggregate materials. So the assurance of Cl^{-1} ion in materials for concrete is mandatory [22].

1.3 Characterization techniques

1.3.1. X-Ray Powder Diffraction. It is an authoritative non-calamitous technique which is used to characterize crystalline materials.[23] XRD supplies data on phase arrangement, textures and other structural parameters for instance crystal defects, strain, crystallinity and grain size. XRD is forthwith a universal characterization approach for determining atomic spacing along with crystal structure. XRD utilizes X-rays for quantifying or investigating crystal structure. XRD is conscious to both the nature or corresponding location of atoms [24].

1.3.1.1. Principle. When monochromatic X-rays hit the crystal lattice, interference pattern is produced. In the vicinity of right distance or angle this interference pattern may be in phase or account constructive interference which is admitted as diffraction [25]. The synergy of X-rays from XRD along the sample outcomes constructive interference when all the conditions fulfill Bragg's law [26]:W.L. Bragg in 1912 remarked that there was a connection betwixt wavelength of radiation, angle of X-rays along with internal spacing in the crystal. This relation is shown as:

$$n\lambda = 2d sin\theta$$

Where integer is expressed by n, wavelength of X-ray is represented by λ which is 1.545Å for Cu source, d expresses the spacing betwixt the planes in the atomic lattice or θ expressed the diffraction angle in degrees. The bigger the wavelength the larger theθ, smaller the distance larger the θ. It is observed that whenever the-rays encounter matter they are slightly transmitted along with partially absorption [26]. Figure 1.4 demonstrates the Bragg's law.
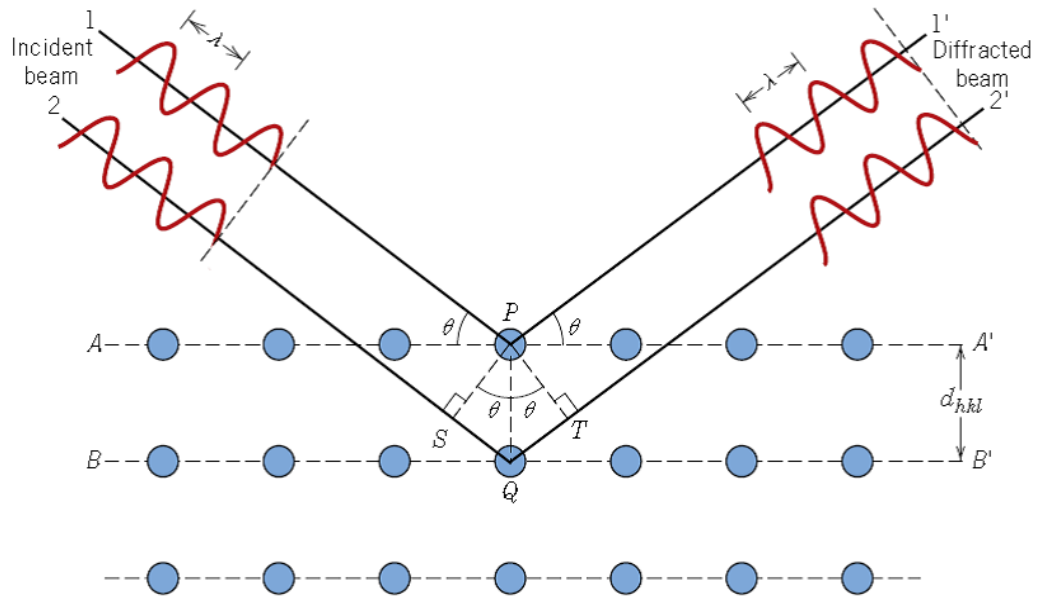
Figure 1.4. Illustration of Bragg's Law [27]

1.3.1.2. Main Parts of Diffractometer. The main parts are discussed below,

a. Source. The source produce X-rays for analyzing sample, typically it is an X-ray tube. It subsists of an empty glass and ceramic vessel that have filament made up of tungsten, which give off electrons called cathode along at which these electrons are accelerated by a potential of certain ten thousand volts called anode.

b. Primary Optics. It regulates the beam outturn by X-rays. This part employs this beam in to the form which is more advantageous for diffraction. It has three segments including Divergence, soller slits along with monochromator.

c. Sample Holder and Stage. It is horsed above the sample stage. Sample stage manages the specimen fixed in a right position. It retains the complete alignment of the beam and manages the displacement of sample.

d. Secondary Optics. Retrieve the X-rays which are diffracted from the sample. It has four parts antiscatter, soller slits, receiving slits, secondary monochromator

e. Detector. It allows the diffracted X-rays to detect. The geometry of an XRD permits the sample to rotate in the avenue of collimated X-ray Detector is horsed on an arm to assemble these diffracted rays and revolves at an angle 2θ. Goniometer is a gadget which is used to retain an angle along with to rotate the sample in the diffractometer. [28]. Figure 1.5 is showing the XRPD.
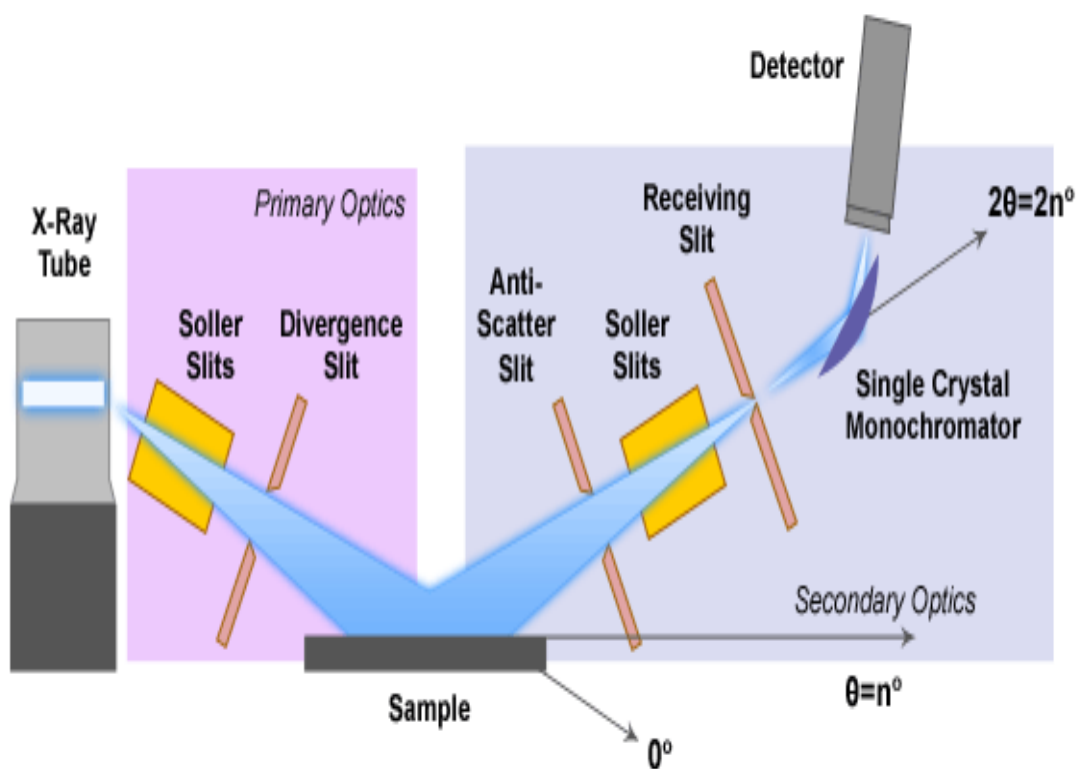
Figure 1.5. Schematic diagram of X-ray Powder Diffraction [29]

1.3.1.3. Sample preparation. Sample should be finely ground (45μm) to get good signal-to-noise ratio and to minimize preferred orientation. It can be done either through mechanical grinding or hand grinding [25].

1.3.1.4 Strengths and Limitations. This technique provides univocal mineral finding, requires minimum sample preparation, provides explicit results along with being quick and emphatic method [28]. If we consider its limitations, than we can say that it demands the accession to standardize file of all compounds and high angle reflections get upset due to peak sheathing [28].

1.3.2 Scanning Electron Microscopy (SEM)

A powerful magnification instrument that employs centered and focused beam of electrons to prevail information. In research & industries it is used to incur

morphology, topography, high resolution 3-D images and compositional information [30].

1.3.2.1. Sample- electron interaction. When the high energy beam of electrons hits the sample surface depending on an accelerating voltage and density of specimen, it perforates the specimen. Many signals are produced like scanning electrons back scattered electrons and characteristic X-rays. Detector collects the signals to form images, displayed on screen. Multiple factors are responsible for maximum SEM resolution i.e. spot size of electron and interaction of beam of electron with specimen. Modern SEM provides resolution between 1-20nm, while it cannot provide atomic resolution [31]

1.3.2.2. Instrumentation. There are two main parts of SEM

a. Electronic console. It is an operational unit the console provides the knobs and switches for adjusting imaging intensity, focus and magnification.

b. Electron optical column. Where beam is generated, focused and scanned across specimen.

c. Electron gun. The source of electron is located at the top of column, it is the part from where the electrons are emitted from hot tungsten filament. Electron gun has three components

      i.   Tungsten filament: it is heated resistively to produce electrons.

      ii.   Wehnelt: it controls the number of electrons.

      iii.   Anode: which accelerates the electrons.

d. Lenses. Condense lens is located below the electron gun and above the aperture. This lens reduce the diameter of the induced electron beam.

Objective lens reduce the coming probe in order to produce a focused image.

e. Scanning coil. When an electron beam is fixated, then scanning coils are utilized to avert an electron beam in the XY axis. It examines in a raster mode over the sample surface. Coils regulate beam position along with scan the beam for image production. It decides the image magnification and fix a probe for X-ray analysis.

f. Sample chamber. Samples are placed and mounted in to a chamber. It has a range of appliances to facilitate in imaging the specimen i.e. translation stage, rotation appliances, and tilt. Optical cameras, introduced through to the exterior along with the temperature stage etc. vacuum is mandatory because electrons can travel only a short distance in air.

g. Detectors. This collect the electrons ejected from the specimen. Secondary and back scattered electrons are the sorts of electrons which are utilized for imaging.

   i.   ***Secondary Electron Detector.*** These are low energy electrons ejected from innermost K shell of the specimen atoms.

   ii.   ***Back scattered Electron Detector.*** These highly energetic electrons are elastically backscattered aside the atoms of those specimen atoms which have high Atomic No (Z). This detector gives compositional information about the sample [32]. Figure 1.6 is showing scanning electron microscope.
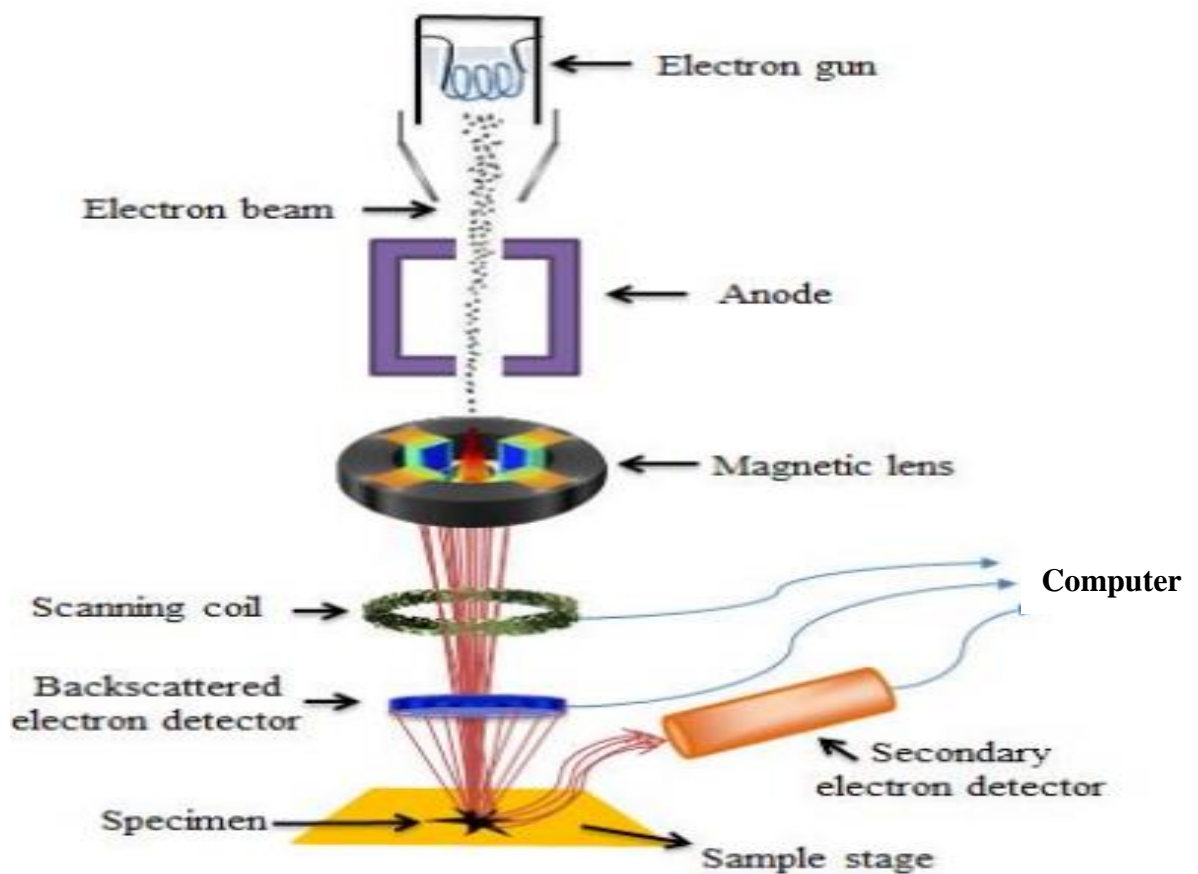
Figure 1.6. Schematic diagram of scanning electron microscope [24]

1.3.2.3 Sample preparation

The sample must be conductive. The surface of sample should be exposed and It must be unwaveringly attached to specimen mount [26].

1.3.2.4 Advantages & Disadvantages

Versatile information earned from different detectors. SEM works fast i.e. SEI, BSE and EDS analysis is less than five minutes. SEM samples requires minimum preparation actions. Digital form of data is generated in the modern SEM [31]. These

are large, expensive and should be honored in a place which may not contain any achievable magnetic, vibration and electric obstruction. The sustenance required i.e. constant current, voltage along with dissemination of chilly water. To prepare sample and to operate SEM special training is required. SEM are limited to solid, inorganic samples etc. Slight hazard of radiation vulnerability correlated with the electrons, because the specimen chamber is configured to forbid any electrical along with magnetic obstrution which should eradicate fluky of radiation outflow the chamber [31].

1.3.2.5 Applications

It provides topography, morphology, compositional information and qualitative chemical analysis with broad range of magnification and resolution up to 1 nm. It Provides information in micro structures. SEM can also detect and analyze surface fractures. It examine surface contamination, identify crystalline structures and reveal spatial variations in chemical composition [31].

1.3.3 Atomic Force Microscopy (AFM)

AFM is one sort of SPM. SPM are configured to measure parameters like magnetism, height and friction with a probe [30].It is the most potent or versatile microscopy appliance. It administers diverse types of measurements of surface, three dimensional topography. It needs minimal sample preparation [33].

1.3.3.1 Principle

The AFM subsists of a cantilever having a pointed tip at end which is worn to scan sample surface. The tip is brought into adjacency of a specimen surface, forces betwixt sample and tip lead to a deviation of the cantilever conferring the Hook's law.

a.   Surface sensing. It has a cantilever having a piercing tip to scan over specimen surface. The tip access the exterior surface, force between the tip and surface cause the cantilever to avert towards the exterior surface. When the cantilever is brought adjacent to surface Repulsive force becomes dynamic, such that tip makes association with it, this phenomenon causes cantilever to avert aside from the exterior.

b.   Detection method. Laser beam is utilized to observe cantilever divagation towards and aside from the exterior. Incident beam is reflected from horizontal top of cantilever. Its tip passes over an exterior, resulting cantilever deflection or the modification in the direction of reflected beam is certified by PSPD.

c.   *Imaging.* Topography of a sample can be viewed via scanning the cantilever over an area of concern. The deflection of cantilever depends upon the raised and lowered features on the sample surface, then it is monitored by PSPD. The height of tip above an exterior can be controlled by utilizing feedback loop, thus it maintains the consistent laser locality. It produces an authentic topographic map of the exterior features [34]. Figure 1.7 is showing the schematic diagram of AFM.

1.3.3.2. Advantages & Disadvantages

AFM provides 3-D surface profile. Samples do not need exclusive treatments for instance carbon coating etc. It may work utterly in an ambient air or liquid environment and does not require an expensive vacuum environment. It may administer more advanced resolution than SEM [35]. But AFM has a single scan image size and limited scanning speed. There is a feasibility of image artifact, which could be generate by an unsuitable tip, even by sample itself and a poor operating environment. [33].
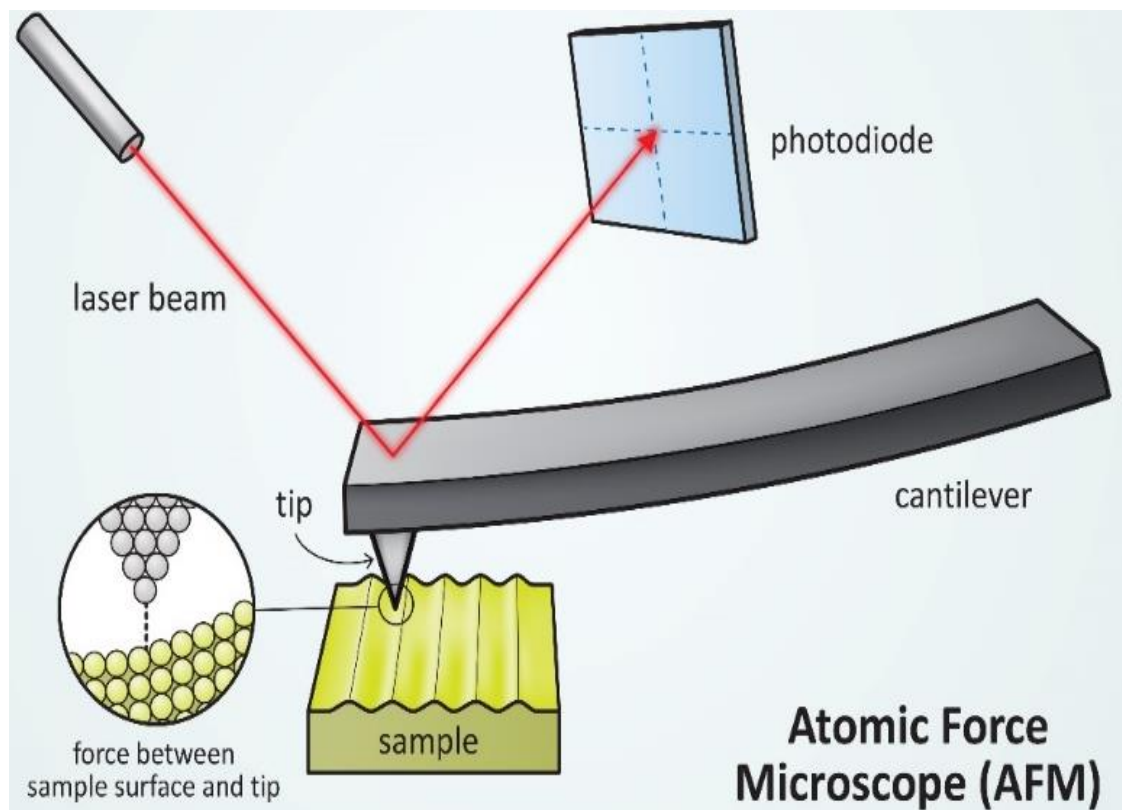
Figure 1.7. illustration of AFM [33]

1.3.4 Brunauer Emmet and Teller (BET)

This technique is appropriate for non-porous materials (for surface area measurement) and porous materials ranging from the microporous (such as MOFs and zeolites) with pores <20 A°, through macropores of around 1000A° [36].

1.3.4.1 Nitrogen Adsorption/ Desorption. When gas molecules come in impinging with some solids, they will compile on the surface of solid and form adsorption layer, this process is called gas adsorption. In a sorption experiment, a familiar quantity of gas is intromit to a restrained volume enclosing the adsorbent. The adsorption process is relegated as chemisorption and physisorption. Chemisorption is based on fundamental interaction of covalent bonding, which is a slow reaction and irreversible process. On the contrary there is a weak van der Waals forces betwixt adsorbent or adsorbate in physisorption, this process is fast, reversible and there is no chemical reaction. Gas sorption measurements are used for ascertaining the pore size, volume and area. Nitrogen adsorption at boiling point of nitrogen 77K, is usually performed to analyze mesoporous metal oxide materials [37].

1.3.4.2 Sample preparation. It is mandatory to withdraw vapours and gases that become physically adsorbed over the sample after storage, handling at the same time as treatment along with manufacturing. If outgassing is not accomplished, surface area must be variable and reduced. The outgassing conditions may be defined by time, temperature and pressure must be selected in case original exterior of solid is reproduced as nearly as conceivable [38]. Care must be engaged when outgassing powder specimen utilizing high temperature to obviate affecting the integrity of sample and nature of surface. Outgassing of many materials is often accomplished by applying an adsorption desorption cycling method, by absolving the sample in a running stream of non-reactive dry gas and by administering as vacuum. If heating is occupied suggested time and temperature of outgassing must be as low as feasible to attain consistent measurements of the surface area in a satisfactory time [39].

1.3.4.3 BET Theory. Irving Langmuir in 1916, presented the Langmuir adsorption equation. This expresses relationship of gas pressure concentration of adsorbate and molecules adsorption on a solid exterior at a settled temperature.

$$\theta = \frac{\alpha \cdot P}{1 + \alpha \cdot P}$$

θ Shows percentage coverage of surface. P represents gas pressure concentration.

α is constant [36]. In 1938, Brunauer, Emmet and Teller put forward a "multimolecular adsorption theory". This theory has three assumptions 1. There is no reaction between each adsorption layer. The first adsorption layer is physical adsorption and multimolecular adsorption is possible. The solid surface is regular [36]. The BET adsorption equation is expressed as following,

$$V = (V_m Cp)/((P_0 - P) [1 + (c-1)P/P_0])$$

Where P represents equilibrium pressure of adsorbates, P_0 is saturation pressure of adsorbates, V demonstrates adsorbed gas quantity, V_m represents monolayer adsorbed gas quantity and c is the constant. By using adsorption equation, adsorption is described through isotherms. Different structure of adsorbent can be determined by adsorption isotherm [40].

1.3.4.4 Types of Adsorption Isotherm. Adsorption heat, structure of adsorbent and other physicochemical properties are the parameters on which adsorption isotherm depends. The adsorption isotherms can be achieved at an expanded range of relative pressures and a consistent temperature. There are six types of adsorption isotherms. Figure 1.8 is showing the different types of adsorption isotherm.

Type I: the materials with type I isotherm are microporous having exposed surface. They, leave little or no extrinsic surface for additional adsorption if once replete with adsorbate. This adsorption limited to one monolayer [41].

Type II: this adsorption isotherm develops on non-porous samples or materials having diameter dominating micropores. On the completion of first monolayer, inflection point occurs [42].

Type III: this isotherm formed due to multilayer adsorption. It is related to the strong interaction of adsorbate- adsorbate and weak interaction of adsorbent-adsorbate. It is identified by adsorption heat which is less than liquification heat.

Type IV: it occurs on porous adsorbents having pores in the range of 1.5 to 100 nm. This isotherm with hysteresis loop is typical isotherm showing a mesoporous materials. At elevated pressure the slope demonstrates enlarged uptake of adsorbate as pores become repleated, inflection point consistently develops nearby finalization of first monolayer.

Type V: this isotherm is detected when there is a limited interaction potential between adsorbate and adsorbent (identical to type III) and are also correlated with pores in the range of 2- 100 nm

Type VI: this adsorption expresses the multilayer adsorption. This isotherm is rare [36].
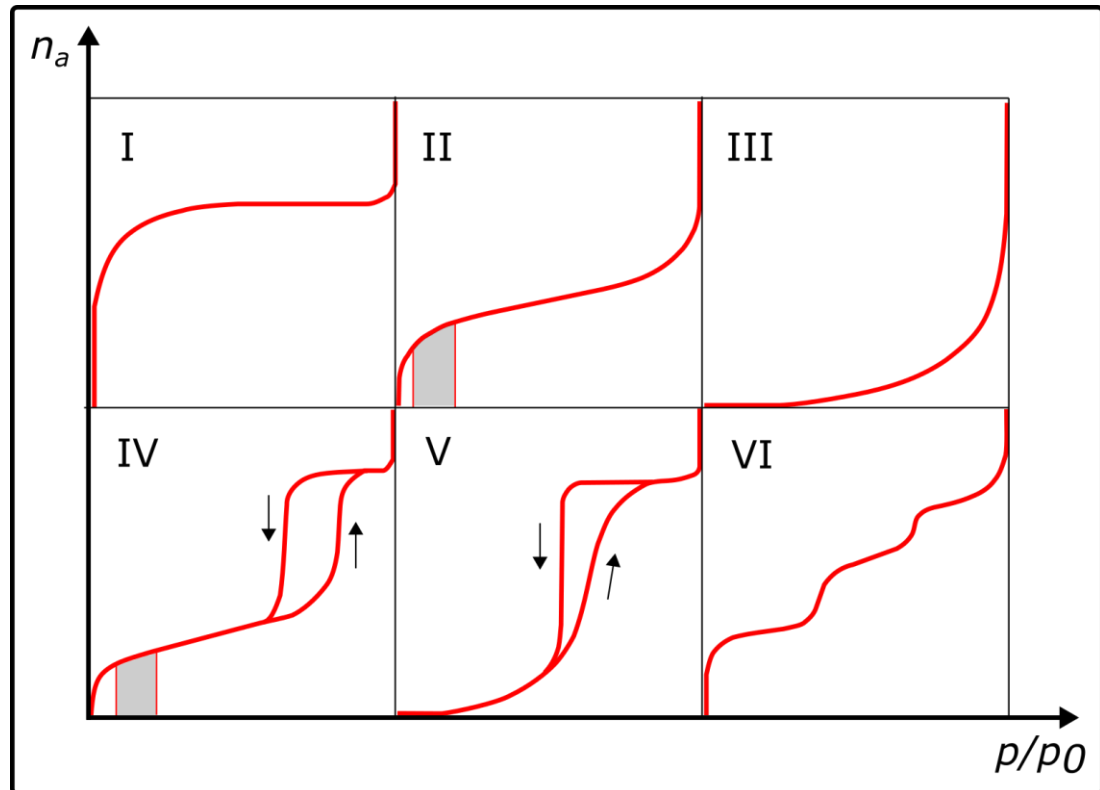
Figure 1.8. Illustration of Adsorption isotherms [36]

Adsorption isotherm is used in many fields and industries for instance, Pharmaceuticals, cement, filtration, ceramics, fuel cells, construction material, paper, medical implants, aerospace, catalysis and geosciences [42].

1.3.5. LCR METER

The LCR meter is an electrical test instrument utilized to measure capacitance (C), inductance (L), and resistance (R) of circuits and components at diverse frequencies. Apart from illustrating these electrical attributes, LCR meters can also generally exhibit quality factor (Q), impedance (Z), phase angle (θ), dissipation factor (D), and equivalent series resistance (ESR). Some LCR meters array admittance and its components and conductance [43]. The LCR meter measures the impedance of the circuit at its terminals, usually compassed by administering a sinusoidal waveform at

a stated frequency and measuring the emerging sinusoidal current ahead with the phase difference between the resulting current and applied voltage. It determines the impedance from these assessments. As circuits and electrical components arrive in a range of pattern, various fixtures and leads are required in alliance with the LCR meter to concede a physical association between the LCR meter and device under test (DUT). As these fixtures/leads also have impedance, it is influential to reimburse for them to recognize the accurate impedance of the DUT [44].

1.3.5.1 Impedance. Electrical Impedance (Z) is the absolute aversion that a circuit presents to interspersing current. Impedance alters inferring to the factors in the circuit and the frequency of the practiced AC. Impedance can comprise resistance (R), inductive reactance (X_L).along with Capacitive reactance (X_C) Inductive reactance and capacitive reactance are 90° out of phase with the resistance, so that their superlative values occur at distinctive times. Therefore, vector addition must be utilized to measure impedance. For AC, Impedance, $Z = \frac{V}{I}$ [44].

1.3.5.2 Capacitance. A capacitor is a passive component with two terminals that stores energy. So this effect of capacitor is acknowledged as capacitance. Capacitors encompass at best of electrical conductors separated by a dielectric medium.in the form of metallic plates Capacitors are categorized in consonance to their dielectric material, which have a range of capacitance values in agreement with their dielectric allocation. The value of capacitor is directly proportional to the current flowing [23].

1.3.5.3 Resistance. Of the three fundamental circuit components, resistors, inductors and capacitors, resistors account the minor measurement obstacles. This is genuine because it is factual to measure resistors by administering a DC signal or at comparably low AC frequencies. In contradiction, inductors and capacitors constantly experience AC signals that by their nature are decumbent to variation, thus these components are ordinarily measured under dynamic circumstances. Resistors are generally measured at low frequency AC or DC, where Ohm's law awards the authentic value under the expectation that loss factors are regarded for [45].

1.3.5.4. Applications. LCR meter is used for fault finding in electrical devices. It can be used to find quality factor, tan loss (tanδ), dissipation factor, and dielectric properties of the material [24]. Figure 1.9 is showing the Block diagram of LCR circuit.
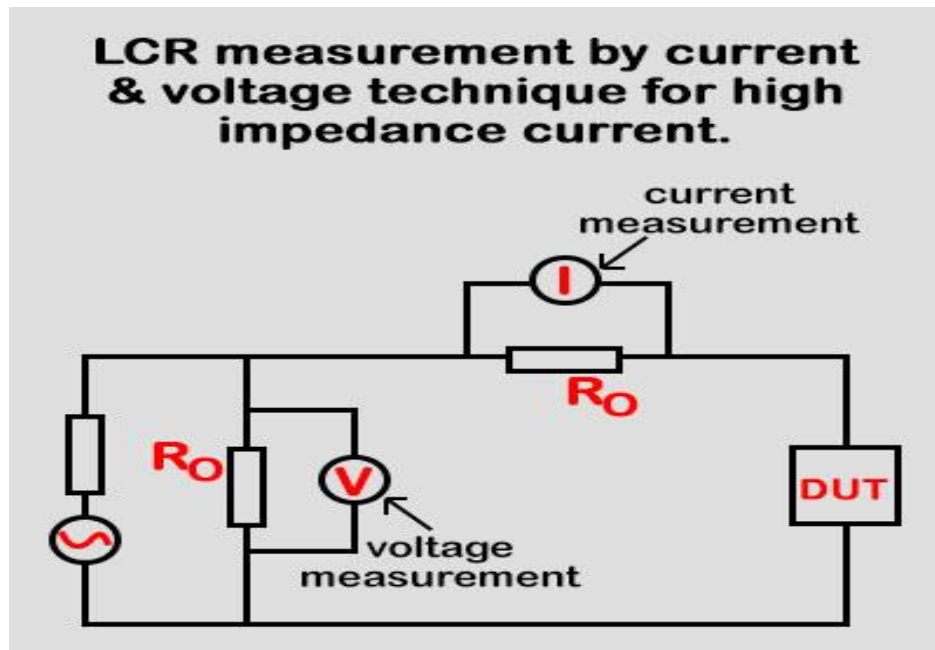
Figure1.9. Block diagram of LCR circuit [44]

1.3.6 Interdigitated Electrode

IDEs (interdigitated electrodes) are prominent transducers, extensively occupied in distinct analytical along with technological functions, exclusively in the field of chemical or biological sensors with low cost, excellent sensitivity and content of fabrication proceeding. Interdigitated capacitors (IDCs) or Interdigitated electrodes (IDEs) are the universally engaged repeated electrodes composition; since their initiation [46].

In the early 1970s, they have been broadly utilized in numerous realms, along with the aspect regulation of the curing practices, supercapacitors, inspecting the dielectric properties, manufacturing of electronic parts. Aside in distinction to these, IDEs have also predominantly accomplish in chemical or biological sensors, in which modifications in capacitance and impedance have been evaluate established on the accord betwixt sensitive layer and analyte. IDEs have been utilized in transducers for lab-on-chip (LoC) devices. Their low cost and the miniaturization of electrodes have made the interdigitated electrode as trendy foundation for conspiring sensor appliance. Economical, simple mass-fabrication process along with the ability of utilizing in diverse appliances beyond hefty advances in sensor lay out are momentous assets of these sensors. Commonly aforesaid sensors have used for measuring capacitance, impedance dielectric constant, and mass conductivity. Electrodes contriving from gold have deposited on a silicon substrate [47]. Essentially the design comprises binary

lateral coplanar electrodes having periodical reiteration pattern (length, width, along with electrode spacing). This sort of sensors need dimensioning to escalate the sensitivity of biological measurement [48]. Figure 1.10 is showing the periodic microelectrode used for sensing.
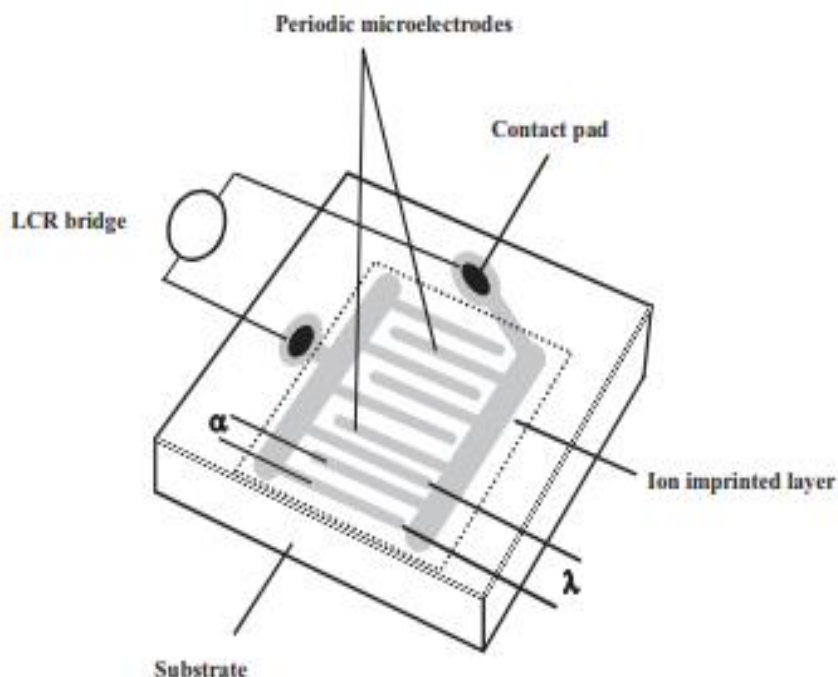
Figure 1.10. Schematic of periodic microlectrodes (PME) device [47]

1.4 Objectives & Motivation

The detailed literature survey led the consideration to the synthesis of templated mesoporous oxides. There has a limited literature available for developing mesoporous oxides utilizing sodium chloride as a template by dint of evaporation method. There was an eagerness to establish an expedient and fiscal methodology for the synthesis of templated mesoporous oxides. Molecular imprinting technology was not used antecedently for the synthesis of inorganic mesoporous oxides utilizing sodium chloride template. Transition metal oxides were not used up to now for the sensing of NaCl.

The preeminent objectives of the research work are given below,

1. To develop an appropriate and monetary methodology for the synthesis of metal oxides.

2. To characterize the product.

3. To check the promising application of the material especially sensing activity.

Chapter 2

Literature Review

Mesoporous and microporous inorganic solids are also utilized as sorption and catalyst media owe to their surface area along with porosity. Exemplary mesoporous materials comprise some sorts of alumina and silica as well as metal oxides and some metals with diverse sets of uniformly-sized porosity [36]. Porous morphology aspects immense attainable exterior areas in consolidation having an associated network of the metal oxide. Mesoporous metal oxide films are utilized in various practices such as water splitting systems, solar cells, electrochromic appliances antibacterial activity, and self-cleaning coatings, etc. [37].

2.1. Porous Materials

The materials which have small ordered and disordered holes are termed as porous materials. Solid and skeletal part of the mesoporous material is termed as "*matrix*" and *"frame"* [49]. Porous materials are divided in to many classes depending on their pore size along with building framework as showing in figure 2.1.
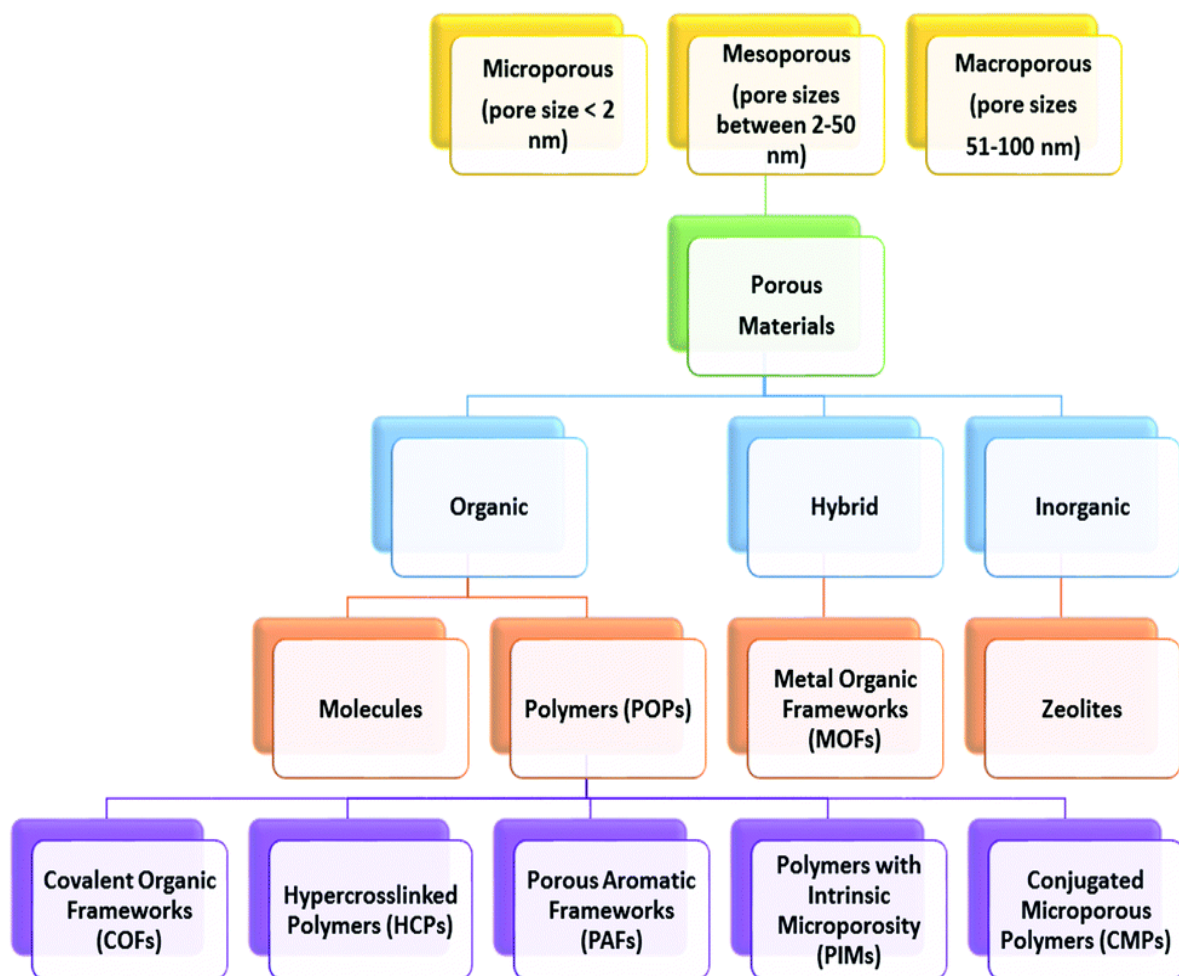
Figure 2.1.Categorization of porous material according to pore dimensions and the nature of the material [4]

2.2. Mesoporous Materials

IUPAC has defined mesoporous materials as the materials which have pore diameter between 2-50 nm [50]. Soon after breakthrough of mesoporous substances in at Mobil Oil Company in 1992 these components are seeking more interest and attention due to having superordinate attributes like; ease of functionalization, surface morphology, tunable pore structure and pore volume, thermal and chemical stability, etc. [51]. Mesoporous materials are divided in to two classes; a) **Silica Based.** These are also termed mesoporous silicates or additionally branched in to two subclasses in which one is composed of pure silicates or another is modified one. b). **Non-siliceous mesoporous material** are further divided in to two types, transition metal oxides and Non-Metallic oxides. Templated mesoporous transition metal oxides are used in many fields and industries owe to their exceptional properties like immense surface area i.e. ZrO_2, TiO_2, MnO, Fe_2O_3, NiO and CuO etc. In **Non-metallic oxides** the templated

mesoporous materials that are not based on silica and metals are formed. These oxides have high surface area and can be used in many fields like catalysis, energy storage and sensors i.e mesoporous carbon, phosphate and sulphate. In which Mesoporous carbon is an intriguing material due to its few exclusive attributes i.e. chemical inertness, hydrophobic nature, and good mechanical and thermal stability. Porous carbon may be prepared via nanocasting method by silicate as a template. These mesoporous carbons due to their transition state theory can be used as a catalyst. But these porous carbon can be collapsed during synthesis, they are not stable, synthesis techniques and calcination are also perplexing. So mesoporous transition metal oxides are more famous due to their thermal and chemical stability.

2.3 Synthesis methods

Mesoporous materials may be prepared by diverse methods including, Chemical etching, Sol-gel method, Microwave and Template assisted technique.

1. Chemical Etching. In this procedure the hollow mesopores are produced on the basis of structural differences between core and shell. Etching takes place by the use of appropriate etchant. while the outer shell remains intact and hollow mesoporous structure formed within the shell [52].

2. Sol-gel Processing. Various morphologies of mesoporous materials may be obtained via sol gel method. General chemistry of this method involves hydrolysis followed by condensation of metal alkoxides and formation of corresponding oxides [53].

3. Microwave-Assisted Technique. At present accessible microwave technology allows the application of temperature-programmed microwave assisted synthesis of mesoporous inorganic materials [54]. Microwave radiations persuade a homogeneous and rapid heating of the sample [55] but still this technique is at introductory [56].

4. Template-Assisted Method. This method is the most popular method because surface area and size of pore may be easily controlled by using structure directing agent or template. An etchant is needed to get mesoporous hollow framework, which may upset the structure of pore [57]. Figure 2.2 is showing the synthesis of imprinted nanomaterials.
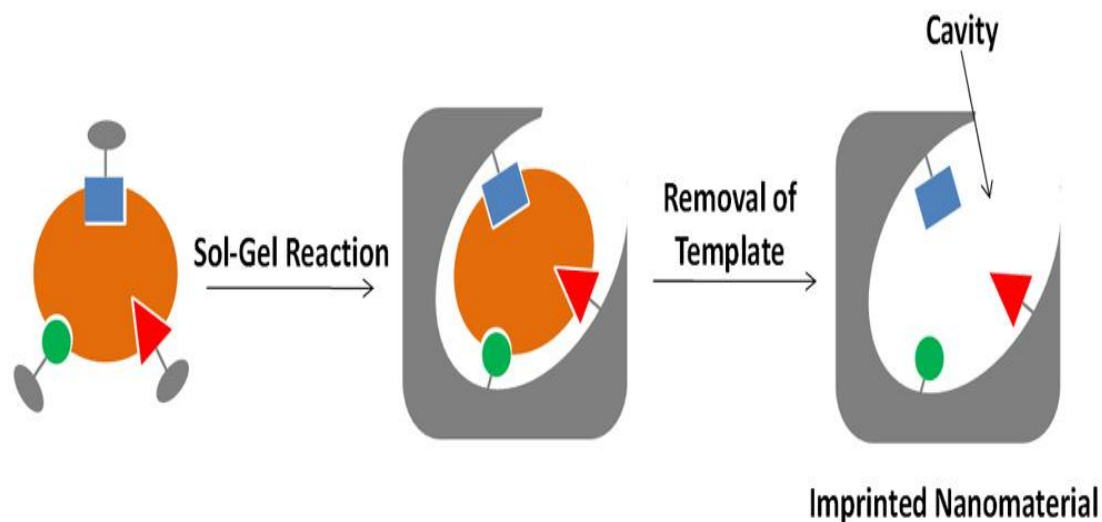
Figure 2.2. synthesis of imprinted nanomaterial [58]

2.4 Classes of Templates

On the basis of template being used, materials can be templated by two ways; exotemplate and endotemplate route.

2.4.1 Exotemplate Method. Exotemplate ('exo' means outside) is also termed as nanocasting method where a porous solid like carbon or silica consistently polystyrene beads, colloidal silica etc. is utilized as the template. Hence, this method is likewise acknowledged as hard-templating or "hard-matter templating". In this situation template remains exterior to inorganic material and hollow space that contributed by the exotemplate structure (generally mesoporous carbon and silica) are replete with inorganic precursor, which is then revolutionized (cured) under applicable circumstances. In this situation, pore system of template is transcribed as "negative image" in the constituent. The now-filled exotemplate is detached by high temperature or by NaOH and HF solution. Later exile of template structure, assimilated substance is achieved with an extensive surface area [9]. Figure 2.3 is showing the schematic representation of exotemplate method.
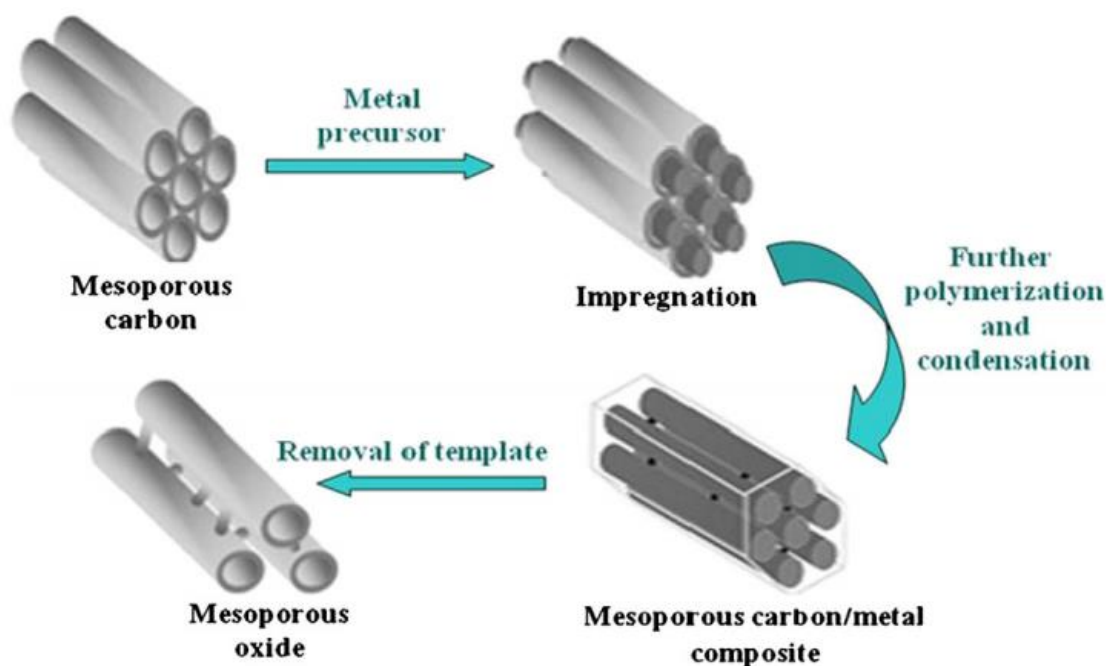
Figure 2.3. Schematic representation of 'exotemplate' method [9]

2.4.2 Endotemplate Method. It is the soft material templating strategy. This is a method in which surfactant or structure directing agent is utilized as a template for preparing ordered mesoporous substances [56].

2.5 Choice of Template. The general route for synthesizing hollow mesoporous metal oxides depends on the disciplined deposition of materials on to removable templates. Templates such as cuprous oxide, polystyrene and silica have been prepared in advance and removed by thermal decomposition and chemical etching. Therefore these methods are usually costly, tedious and less stable due to multistep strategies comprising formation of template, shell deposition then at the end eviction of template [59]

Formal generation of mesoporous framework is generally carried out either via soft or hard template. Hard template depends on the utilization of pre-shaped solid materials of ceramic and polymeric compound like SiO_2, polystyrene and $CaCO_3$. In the hard template strategy, target or precursor is initially coated on to hard template or surfactant and then hard template is detached by either chemical etching or firing to leave the target substance being porous or hollow. But this method of template removal is costly and complicated and attended by the spillage of environmental hazards [60].

2.5.1 Advantages of Using NaCl as a Template. The removal of template by rigid access like HF, organic solvent and NaOH brought the feasibility of material damage. A facile approach to synthesize mesoporous metal oxides using NaCl crystal as a template was introduced by Rui Liu. So sodium chloride is a water soluble salt, getting rid of this template is elementary than metal oxides owe to greater difference in water solubility betwixt oxides and ionic compound. Sodium Chloride is a crucial constituent with great copiousness. It has prevailed in all living organisms from ancient time [61]

Sodium chloride is also known as table salt with molar mass 58.445 g/mol. It consists of Cl^{-1} as an anion and Na^{+1} as a cation. It has crystalline framework in which each Na^+ ion is surrounded by six Cl^{-1} ions to give an octahedral geometry. It has a FCC crystal structure with a lattice constant 564.02 pm [62]. Figure 2.4 is showing the crystal structure of NaCl.
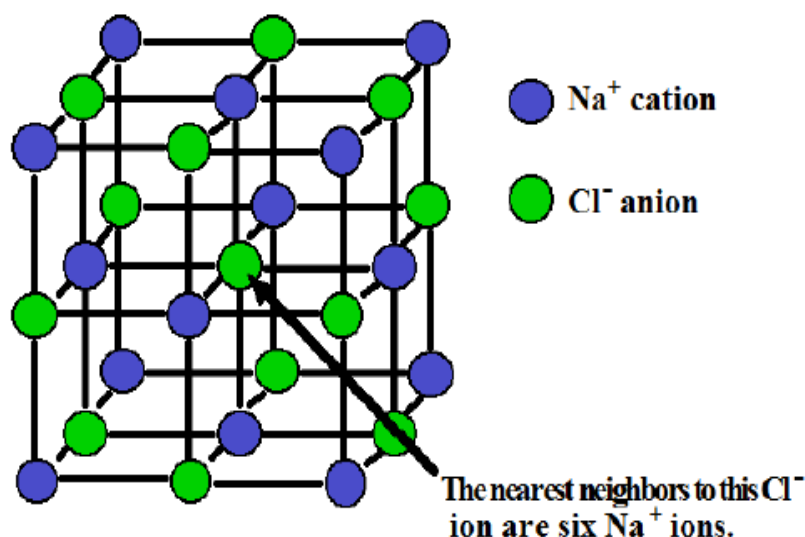
Figure 2.4. Shows the structure of NaCl [63]

It is white crystalline material with a density of 2.16 g/mol. It has a M.P of 801°C. It is transparent to translucent cubic crystal, also granular or powder [63]. It is utilized in preparation of bounteous essential chemicals such as baking soda, NaOH, Na_2CO_3 and HCl etc. NaCl is also used in textile industry, rubber, paper and pulp industry fire retardants and oil refineries along with in road construction. It is also used in de-icing of side walls and roads in snowy and cold regions. It is used in the medical field too [64].

2.6 Transition Metal Oxides as a Target Material

These are the compounds composed of transition metals obligated to oxygen atoms. They are commonly used for their semi conductive properties and catalytic activity [65]

2.6.1 Monoxides. Many compounds from the first row of transition metal form monoxides i.e. from TiO to NiO. These monoxides have a rock salt cubic structure. This halite structure is generated by filling all the octahedral sites with a cation in an oxygen anion FCC array [66]

2.6.2 Defect Sites. In rock salt surfaces, metal, metal cation and oxygen vacancies are the most common point defects. These oxygen vacancies are produced by annealing to high temperature and electron bombardment. Oxygen vacancies have a greater impact and are more common than vacancies of metal cation. These oxygen vacancies affect the electronic energy level. The two other common defects in the rock salt surfaces are kinks and steps. These defects reduce the coordination of the cations from 5 to 4 [67].

2.7 Some important Transition Metal Oxides

Metal oxides show a crucial aspect in many fields of chemistry, material science along with physics. These metal elements are adept to design a considerable diversity of oxide compounds. These may endorse a broad number of structural geometries with an electronic framework that can display metallic, semiconductor insulator aspect. In technological functions, oxides are worn in the fabrication of microelectronic circuits, piezoelectric appliances, coatings for the passivation of areas across erosion, sensors, and catalysts along with as fuel cells. Figure 2.5 is showing the crystal structures of NiO, CuO, Fe_2O_3 and Co_3O_4.

2.7.1 Nickel Oxide. Nickel (II) oxide has the formula NiO. It is only the well-known oxide of nickel. It is classified as basic metal oxide. It is green crystalline solid in appearance. It is insoluble in water with a melting point 1955°C. Its density is 6.67 g/cm^3 [68]. NiO has the halite (NaCl) structure with an octahedral Ni^{2+} and O^{2-} sites [69]. Nickel oxide is used as a Gas and temperature sensors such as CO, H_2 and formaldehyde sensors etc. it is used as a Catalyst, as a counter electrode, as Adhesive and coloring agents for enamel, as Active optical filters, as a Cathode substance for

alkaline batteries and as a Pigment for glasses and ceramics. It is also utilized in Electro chromic materials and in Antiferromagnetic layers [70].

2.7.2 Copper Oxide. Copper (II) oxide or cupric oxide has the formula CuO.it is also known as tenorite. It is black in color [71]. It belongs to monoclinic crystal system in which copper cation is bounded by four oxygen atoms to give square planar geometry. It is insoluble in water with a band gap of 1.2 ev. Its melting point is 1326°C [72]. CuO is used as a Chemical sensors, Efficient Antimicrobial agent, and Optical glass polishing agent, Ceramic resister, super conducting and thermoelectric material. It is also used as a pigment Galvanic electrode or energy storage batteries or cells and as a catalyst [73].

2.7.3 Cobalt Oxide. Cobalt oxide is a white powder. It is insoluble in water with a melting point 895°C [74]. It has a spinel crystal structure. In this structure Co^{3+} are present in the octahedral interstices whereas Co^{2+} in the tetrahedral interstices of the cubic closed crystal system. They are p-type semiconductor with an important magnetic properties [75]. Cobalt oxide is used as a temperature and gas sensors, in enamels, as energy absorbers and grinding wheels, as carbides, in microelectronics, as a Chemical industry oxidants, in catalysis, in electronic ceramics and as superconductors, in Senior googles ,in filter materials and as a Chemical industry oxidants [76].

2.7.4 Iron Oxide. The chemical formula of ferric oxide is Fe_2O_3. It is also known as hematite. It is a dark red ferromagnetic material and can be easily attacked by acids. It is also called "Rust" and is acidic in nature. It is insoluble in water. Its melting point is 1539-1565°C [77]. Its coordination geometry is also octahedral, in which each iron center is surrounded by six oxygen atoms.Fe_2O_3 has three phases: Alpha-form which is rhomohedral and most common form. This form is antiferromagnetic below 260K.Beta form is cubic body centered, metastable state, at 500°C converted to alpha form. Gamma form is cubic spinel, metastable state and converted from alpha form at higher temperature. This form is ferromagnetic in nature [78]. Iron oxide is used in many fields and industries i.e. as a Sensors, Iron industry, Polishing Pigment, Magnetic recording, Photocatalysis, Medicine, Superparamagnetic relaxometry and High sensitivity bimolecular magnetic resonance imaging (MRI) [79].
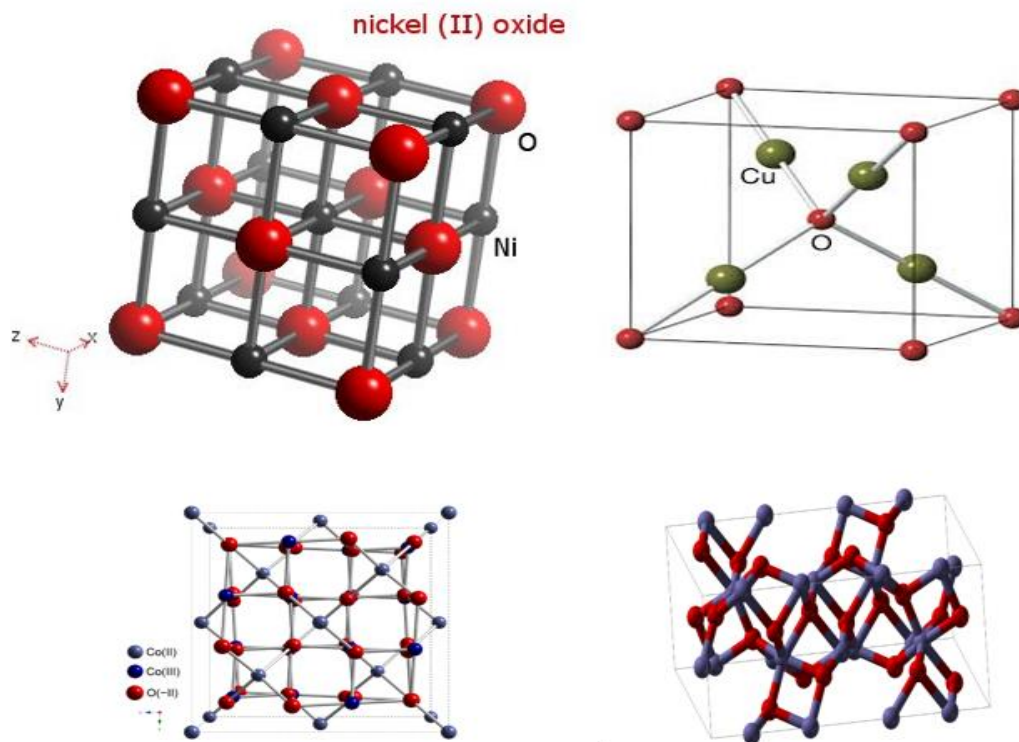
Figure 2.5. The crystal structure of a) NiO [80] b) CuO [81] c) Co$_3$O$_4$ [82] d) Fe$_2$O$_3$ [83]

2.8 Molecular Imprinting in Transition Metal Oxides by using different Templates

2.8.1 Carbon as a Template. Maria-Magdalena Titirici prepared hollow sphere of crystalline metal oxides, (Fe$_2$O$_3$, NiO, Co$_3$O$_4$, CeO$_2$, MgO and CuO) in a simple one-pot synthesis via a hydrothermal approach. Various metal salts were dissolved together with carbohydrates in water, and the mixture were heated to 180°C in an autoclave. Carbon spheres were formed with metal ions merged in to their hydrophilic shell. Hollow metal oxides were formed after the removal of carbon via calcination. Instead of fabrication by multistep process that includes the formation, isolation, purification of carbon spheres, coating of core with the metal oxide precursors and then removal of carbon core by calcination, this method combine metal salts straightly to the carbohydrate solution in water, followed by hydrothermal treatment. Lower metal content tracked to a light packing of metal oxide nanoparticles and a thin shell, whereas an increase in metal content produced a racy, thicker shell and a much denser packing. The materials were characterized by XRPD. The morphology and particles size was

anticipated by utilizing SEM and TEM. Surface area was determined by using BET [84].

2.8.2 Carbonaceous Polysaccharide as a Template. Xiaoming Sun synthesized metal oxide hollow sphere by utilizing carbonaceous polysaccharide microspheres as a template. He prepared these microspheres from a saccharide solution via dehydration under hydrothermal circumstances. The exterior of these materials was hydrophilic and functionalized with Hydroxyl and Carbonyl groups, or was identical in configuration to polysaccharide. At the time of diffusion of carbonaceous microspheres in metal salt solution functional group in the exterior layers were adequate to bind metal cations through coordination and electrostatic association. In calcination process the exterior layers assimilating the cationic metal ions were cross-linked to design metal oxide hollow spheres. A serious of metal oxides hollow structures such as main group metal oxides (SnO_2, Al_2O_3, Ga_2O_3), Transition metal oxides CoO, NiO, Mn_3O_4, Cr_2O_3) and rare earth metal oxides, La_2O_3, Y_2O_3, Lu_2O_3, CeO_2) had been prepared in this way. Size of hollow structures was around 40% of the original template. Shells of all metal oxide hollow spheres were consistent, perfect and no more than 20 nm massive. Carbonaceous template determined the configuration and structure of final materials. These hollow metal oxides were used as a gas sensor [85].

2.8.3 PMMA as a Template. Facile method had been introduced by masahiro sadakane to generate three dimensionally ordered macroporous (3DOM) alumina, chromium oxide iron oxide, manganese oxide, and their mixed metal oxides. PMMA was used as a template .heating initiated the nitrate oxidation with Ethylene Glycol to form metal glyoxylate. The nitrate oxidation temperature must be lessened than the glass transition temperature of the PMMA. Heat produced by oxidative decomposition of PMMA should be ejected. In this facile one-pot synthesis method EG- methanol mixed solution of metal nitrate salts were used. At low temperature and before the removal of template these mixed solutions converted to metal glyoxylate or metal oxalate derivatives. Calcination detached the polymer template, the glyoxylate salt transformed to mixed metal oxides with immense porosity (66-81%) was confirmed by Hg porosimetry [86].

2.8.4 Different Soft and hard Templates. Metal oxides also prepared by simple precipitation method utilizing metal salts and ammonia solution. Jin –song Hu

synthesized hierarchically structured metal oxides and used them in heavy metal ion discharge. Uniform morphology was obtained by using soft (CTAB, TBAB, PVP, and block copolymers like P_{123}) and hard templates (carbon and silica). Iron oxides such as Fe_3O_4, α- Fe_2O_3, Υ- Fe_2O_3 were prepared by using **TBAB** as a soft template. Coral or sea worm like SnO_2 substances were prepared by Zhu et al. utilizing **poly-L- lysine** as a template. Co_3O_4 nanoboxes were prepared by using **SDBS** as the template in ethanol medium. In entire specified processes template was dissolved in a solution or form self –assembled micelles that administers framework direction for the metal oxide precursors. Calcination was done to obtain desire crystallinity, but it was a very energy intensive process. Nanoporous TiO_2 was synthesized by this process with an immense surface area of $245.5 m^2.g^{-1}$. The major advantage of these methods were low energy consumption and chemical discharge during the formation of metal oxides. Hard template i.e. **carbon and silica** were used to preset the morphology and porosity. The general methodology for hard template was replete an empty pores of templates with metal oxide precursor, change this precursor in to metal oxide and certainly detach the template via combustion or chemical etching. Hollow TiO_2, Fe_2O_3, Co_3O_4, SnO_2 and MnO_2 were prepared by using **carbon fibers** as a hard template. **SiO_2** having macropores (0.51-30μm) along with mesopores (3.1-30nm) were synthesized and utilized as a hard template. Pores in the SiO_2 were replete with metal salt solutions which converted in to metal oxide under thermal treatment. Finally silica was detached by utilizing Sodium Hydroxide solution [87]. **Egg shell membrane (ESM)** were also used as a template in bio-inspired synthesis process. The ESM provide bio macromolecules as a capping and structure directing functions to produce ordered metal oxide nanocrystals.

2.8.5 NaCl as a Template to form SiO_2 and TiO_2 Hollow Structures. Bing bing Wang reported a new approach by precisely forming templates from Sodium Chloride solutions. Property of templates altered by choosing proper organic solvent and changing crystal growth circumstances. These NaCl templates are ample, water soluble, environmental friendly and uniform in size and geometry. These templates were excellent for synthesizing great quality hollow nano/micro frameworks. Different morphologies were reported by using NaCl as a template in different solutions. RD-NaCl was obtained when Sodium Chloride –glycerol was heated at 140°C and this solution was mixed to a 2-Propanol drop wise. From Thomson-Gibbs expression and

thermodynamic, the exterior of crystal could be controlled by accommodating supersaturation of crystal growth. Small NaCl submicro-cubes were obtained by using 2-butanol as a solvent that has one extra $-CH_2-$ group as compared to 2-propanol. Sodium Chloride – submicro cubes were of around 120nm in size. Corresponding supersaturation in 2-butanol was greater than that in 2-propanol, was leading to greater nucleation rate. Octahedral Sodium Chloride crystals were obtained by aging as-prepared NaCl nanocubes in dry atmosphere for 1day. The SiO_2 and TiO_2 hollow structured particles were obtained by coating them on to NaCl microcubic crystal templates. Entire of the morphologies were the Copy of initial Sodium Chloride template [60]

2.8.6 NaCl as a Template to Form Mesoporous SnO₂. Ruiliu and Shengchun Yang synthesized tin dioxide hollow nanocubes using common salt as a template. Due to high lithiation-delithation capacity of SnO_2, it considered the best known anode material for lithium-ion battery functions. It was appropriate to make SnO_2 porous or hollow structures in the provision of electrode. The removal of NaCl is much easier than oxides owe to greater difference in water solubility betwixt oxides and ionic compounds. SnO_2 crystallinity ameliorated, while hollow morphology remained intact after the annealing.

$$SnCl_4 + NaBH_4 \xrightarrow{yields} Sn + H_2 + NaCl + BCl_3 \textbf{ (1)}$$

$$Sn + O_2 \xrightarrow{yields} SnO_2 \textbf{ (2)}$$
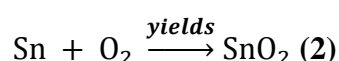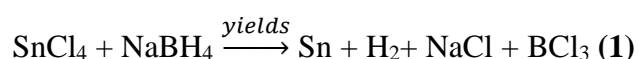
TEM images showed that the average edge length of cubes was between 301 and 500nm. Holes were observed in the individual nanocube. Extra magnified TEM images showed that the shell of hollow cubes was of porous framework. The Formation of hollow cubes occurred in three steps. At the first step NaCl which was formed in situ acted as a template, deposit the SnO_2 small crystallites over its surface. At the second step, these deposited SnO_2 started to attach each other because of the Ostwald ripening. This resulted the creation of shell layer on the exterior of sodium Chloride crystals. Finally NaCl crystals were removed by washing with water [61]. Figure 2.6 is showing the drawing of the creation of hollow cubic SnO_2.
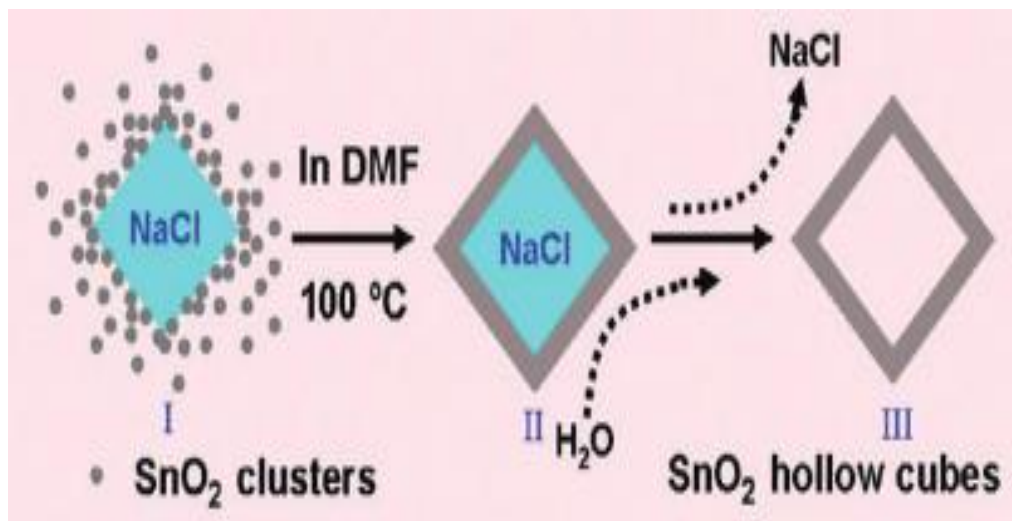
Figure 2.6. Schematic drawing of the formation of hollow cubic SnO₂ [61]

2.8.7 Triblock Copolymers as a Template. Ordered mesoporous silica of SBA-15 and SBA-16 was synthesized by utilizing triblock copolymers as a template. SBA-15 was prepared by using hydrothermal and sol-gel strategy and **pluoronic P₁₂₃** as a template. SBA-16 was only prepared by hydrothermal approach using **pluoronic F₁₂₇ and butyl alcohol** as a template. To detach the template, product was rinsed with an ethanol/HCl mixture. The mesoporous silica was characterized by using XRD, BET and TEM. Hydrothermally synthesized SBA-15 showed the greatest adsorption capacity of biomolecules (BSA, LYS). Whereas the SBA-15 synthesized by sol-gel method adsorbed maximum cellulase. Due to nature of its own structure SBA-16 showed lower adsorption capabilities for all biomolecules (BSA, LYs and CEL). It showed FCC structure with narrow pores [88]

2.8.8 Different Forms of Silica as a Template. An ordered mesoporous silica (**MCM-41, KTT-6, and SBA-15**) were utilized as a template for preparing ordered mesoporous cobalt oxide via nanocasting process. Nanocasting method is appropriate for producing for producing rigid mesostructures with greater crystallinity. The morphology and the pore system was controlled by varying the hard mesoporous silica template [89]

2.8.9 Mesoporous Hollow Carbon as a Template. A hard templating strategy was used by Swasmi Purwajanti to synthesize mesoporous hollow carbon spheres (MCHS) as a template. The carbon spheres were appropriate to using as a template to synthesize many mesoporous metal oxides. During the synthesis of mesoporous metal oxides they

were easily removed by combustion in air. A wet impregnation method was used to obtain mesoporous metal oxide hollow spheres i.e. MgO using MCHS as a template. These mesoporous hollow spheres were used as adsorbent to remove arsenic (As III) from aqueous solution due to its fast removal rate, high adsorption capacity and high efficiency under low arsenite concentration [90]

2.8.10 NaCl and KCl as a Template. Xu Xiao synthesized two- dimensional transition metal oxides by scalable salt-templated method. He synthesized MnO using KCl and hex-MoO_3, MoO_2 and hex WO_3 using NaCl as a template. The planar growth was speculated to come about via a check between the crystal lattice of the growing oxide and the salt. The morphology and the structure of these 2D- transition metal oxides were studied using FE-SEM, AFM, and HRTEM and XRD. These oxides were used as energy storage application [91]

2.8.11 CTAB as a Template. Mesoporous silica nanoparticles were prepared by via sol gel method, using TEOS as a precursor along with **CTAB** as a pore generating agent. The morphology of mesoporous silica had been changed from dispersed nanospheres to agglomerates by increasing both the hydrolysis of TEOS and amount of CTAB. Whereas pore size and pore diameter remained same between 2.5 and 2.8 nm. The addition of CTAB produced silica with high specific surface area ($585m^2g^{-1}$) and pore volume ($0.49cm^3g^{-1}$), due to Ostwald ripening mechanism. The dilution of sol lead silica to form to the formation of rod like particles with high surface reactivity. The mesoporous silica nanoparticles were characterized by using FESEM, HR-TEM, BET, DLS and Zeta potential. These results clearly confirmed that addition of CTAB and the amount of water were strongly impact the porosity and specific surface area of mesoporous silica nanoparticles [53].

• Mesoporous silica nanoparticles (MSN) and nanorods (MSNR) were synthesized by Sahei Rahmani using sol gel process. He used TEOS as a precursor and **CTAB** as a template. The structure and particle shape of mesopores were easily controlled by the addition of ethanol as a co solvent. These mesoporous silica were used in drug delivery and killing cancer cells [92].

• Mesoporus manganese, nickel and iron oxides were prepared by ultra sound assistance using **CTAB** as a template. Ultrasound pretreatment has been applied on the template to make mesoporous metal oxides that owned high specific surface area

and were thermally stable up to 300°C. The morphology and the size of mesoporous metal oxides were easily controlled by changing the temperature of the ultrasound. The annealing of specimen at 300°C ensured the complete removal of template which resulted high porosity and specific area [93].

- Mesoporous silica of the type MCM-41 with varied pH content was synthesized using **CTAB** as a template under hydrothermal conditions. Materials were characterized by XRD, BET and TEM. Thickness of wall, diameter of pore and specific area were 0.8nm, 4nm and 1050-1070 m^2g^{-1}. MCM-41 showed hexagonal symmetry. Results investigated that regularity of crystal structure increased by decreasing the amount of pH [94].

2.8.12 NaCl as a Template to Form Cobalt Oxide Octahedrons. Cobalt oxide octahedrons have been synthesized by a novel template synthesis route using sodium chloride as a template which was formed in-situ during the reaction process. Octahedral NaCl templates has been well formed when its concentration reached over a certain range of saturated solubility. In order to get perfect octahedral templates additional NaCl (0.3g) was added in addition to the NaCl formed during a chemical reaction. Otherwise the products could be the dispersive spherical nanoparticles

$$CoCl_2 + NaBH_4 \xrightarrow{yields} Co + H_2 + NaCl + BCl_3 \quad (1)$$

$$3Co + 2O_2 \xrightarrow{yields} Co_3O_4 \ (2)$$
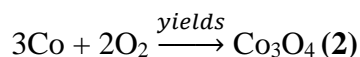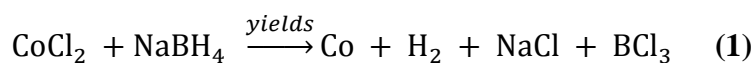
In the first step cobalt oxide small crystallites started to deposit on the surface of NaCl crystal, formed during the chemical reaction which acted as the template. In the second step these deposited Co_3O_4 small crystallites due to the Ostwald Ripening, started to attach each other. As a result on the surface of NaCl crystal shell layer has formed. When solid octahedron particles washed with water, NaCl templates removed while Co_3O_4 has reserved. TEM images confirmed that porous shell of hollow octahedron has composed of ultra-small particles As synthesized Co_3O_4 porous material have superior cycling performance and high capacity [59].

2.8.13 NaNO₃ as a Template. In 2018, Wengeli Li has synthesized a novel sponge-like iron oxide microspheres by a facile aerosol spray pyrolysis method. A reaction between Fe $(NO_3)_3$ and Na_2CO_3 generated the $NaNO_3$ as a fluxing sacrificial template.

$$\text{Fe (NO}_3)_3 + \text{Na}_2\text{CO}_3 + \text{H}_2\text{O} \xrightarrow{yields} \text{Fe (OH)}_3 + \text{NaNO}_3 + \text{CO}_2$$
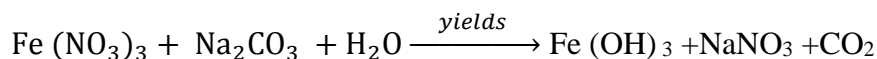
A sponge like Fe_2O_3 microspheres have been formed after the removal of $NaNO_3$ template. The mesoporous Fe_2O_3 has been characterized by using XRPD, XPS, SEM, HRTEM, and BET. High surface area of 216.2 m^2g^{-1} and average pore size of 4 nm has been obtained by utilizing spray pyrolysis method. These sponge like Fe_2O_3 exposed a better catalytic activity for CO conversion at low temperature [95].

2.8.14 NaCl as a Template to form Si Nanosheets. Recently in 2018, the Silicon nanosheets have been synthesized via a scalable and facile synthesis strategy. He used NaCl as a sacrificial template, TEOS as a silica precursor and assisted with a magnesium reduction method. Large surface area of nanosheets have been obtained due to the recrystallization of NaCl via a self-assembly process on the surface of Sodium Chloride. Morphology of Silicon nanosheets have been absolutely preserved by magnesium reduction. Improved rate and cycling performance of these Si nanosheets have been achieved by combining them with the reduced graphene oxide. Reduced grapheme oxide has been prepared by a novel double step microwave radiation method. These 2D Si nanosheets and its composite with RGO have been characterized by using XRPD, XPS, SEM, TEM, along with Raman spectra. Si@RGO composite showed high specific capacity, exceptional electrochemical achievement, superb rate capability and distinguished cycling stability [96].

2.9. Characteristics of Mesoporous Materials

They possess large surface area, capable for sorption process, have higher thermal stability and long range ordered porous structure. By using different surfactants, different morphologies and structures like sheets and rods can be obtained. The pore size dissemination is entirely limited, but by changing the composition of surfactants and chemical composition of synthesis mixture their pore size may be changed from 2 to 30 nm. Porous substances may be ordered if the atoms of host and template have long range ordering. These types of crystalline ordered materials give sharp maxima in diffraction analysis with X-rays, neutrons or electrons [56].

Chapter 3

Experimental

This chapter describes synthesis, characterization and application of non-imprinted and Imprinted mesoporous transition metal oxides using $Ni(NO_3)_2.6H_2O$ (BDH chemicals Ltd Poole England 99.99%), $Cu(NO_3)_2.3H_2O$ (Sigma-Aldrich 99.99%), $FeCl_3.6H_2O$ (Sigma-Aldrich 99.99%), $Co(NO_3)_2.6H_2O$ (Sigma-Aldrich 99.99%), C_2H_5OH (Merck Millipore 99.99%) and NaCl (Sigma-Aldrich 99.99%).

3.1. Synthesis

10g of NaCl was added to 1M Ni $(NO_3)_2.6H_2O$ solution in ethanol under continuous stirring at 70ºC for 30min. The mixture was collected after complete evaporation of ethanol then heated @2ºC/min up to 400ºC and maintained at a final temperature for 1h [91]. The black powdered NiO was homogenized by sonication for 0.5h in DI water. Whereas NaCl template was removed by three times centrifugation @11000 rpm for 20min in DI water at 40°C. As obtained NiO sample was dried at 70°C for 2h. Similar templated method was employed for synthesis of templated mesoporous CuO, Fe_2O_3 and Co_3O_4 from their respective metal precursors. Whole synthesis process is described in the flowsheet diagram given in figure 3.1. In the case of non-imprinted metal oxides same synthesis methodology was followed in the absence of sodium chloride template.
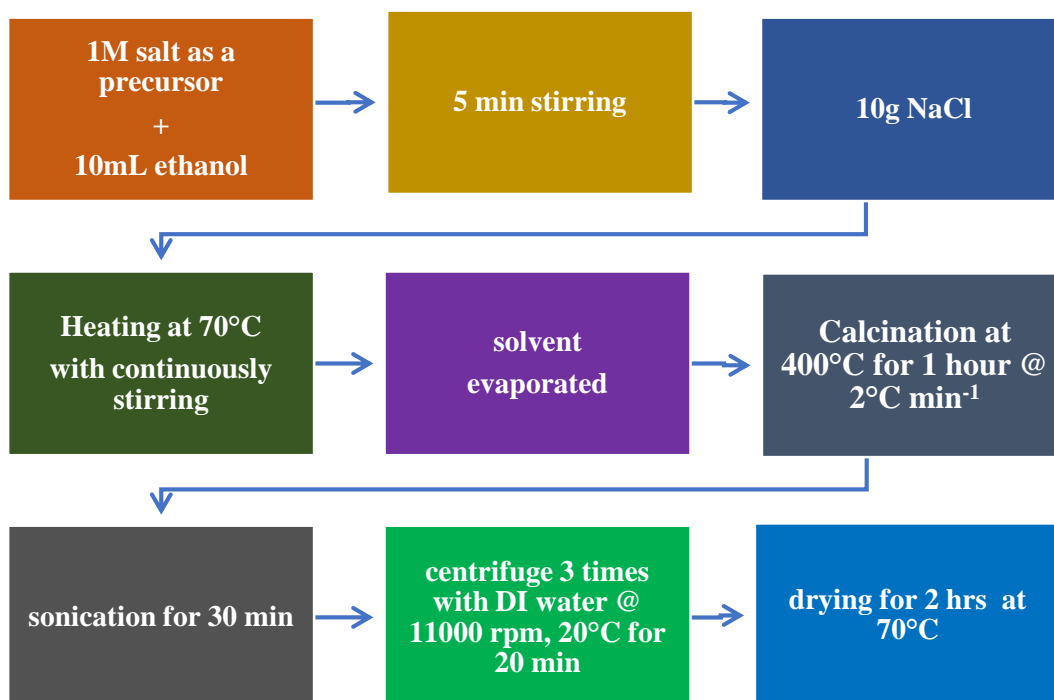
1M salt as a precursor + 10mL ethanol	→	5 min stirring	→	10g NaCl
Heating at 70°C with continuously stirring	→	solvent evaporated	→	Calcination at 400°C for 1 hour @ 2°C min⁻¹
sonication for 30 min	→	centrifuge 3 times with DI water @ 11000 rpm, 20°C for 20 min	→	drying for 2 hrs at 70°C

Figure 3.1. Flowsheet showing the synthesis scheme of imprinted mesoporous oxides

3.2. Characterization

X-Ray Powder Diffraction (XRPD). XRPD measurements of template mesoporous oxides were performed via advance Bruker diffractometer (D8 Discover) working at 40kV with $Cuk_{\alpha1}$ monochromatic radiation, data collected within range of 20°<2θ>80° at a 1°min⁻¹ scan rate and 0.2° step size.

Scanning Electron Microscopy (SEM). The morphological analysis was done via scanning electron microscopy (SEM model VEGA 3 TESCAN) operating at 20kV. The suspension of powder sample was made in DI water and probe sonicated for 30min for homogeneous dispersion. Thin film of suspension was coated over a glass plate and then desiccated for 15min. As the samples were non-conducting so they were Au sputtered.

Brunauer Emmet Teller (BET). Adsorption experiments were performed to ensure pore volume or pore size of the synthesized materials on micromeritics instrument Gemini VII 2390. The glass tube containing 200 mg specimen was heated at 120°C for 1h under vacuum to remove any moisture. Finally glass tube was immersed in liquid N_2 for adsorption/desorption evaluation at 77K.

Atomic Force Microscopy (AFM). This was used for quantitative roughness measurements and imaging the surface morphology. AFM scans were performed in air on dry films. It was used in tapping mode with silicon tips with a resonance frequency around 250 kHz. To make thin film for AFM imaging thin film of sample suspension was applied over a glass plate and desiccated in an oven for 20min.

3.3. Sensing System for Salinity Testing

The experiments were performed with a JET-7600 plus precision LCR meter at a frequency of 1000 HZ. Metal oxide films were utilized as a basic material to establish sensors. Suspensions having 3 mg powder samples were made in 300 μL DI water. Later, these thin films were applied on the interdigital electrode by drop-coating method. This electrode was dried completely by keeping at 100°C for 20min. NaCl was utilized as solute or analyte to establish the salt solutions for salinity check in DI MilliQ® water (Resistance: 18.2MΩcm and pH: 6.71). Electrochemical sensing was used to figure out the sensor feedback during testing with different NaCl content in a range of 5-50ppm. The Cs (series capacitance), Rp (parallel resistance) Cp (parallel capacitance), Rs (series resistance), and Z (impedance) were collected from the LCR meter.

3.4. Selectivity Check

To check the selectivity of mesoporous transition metal oxides 50ppm solutions of NaCl, $CaCl_2$, KCl, NaF and KBr were prepared in DI water. The selectivity was checked from the LCR meter.

Chapter 4

Results & Discussion

This chapter describes the synthesis and characterization of non-templated and templated mesoporous oxides inclusive of the findings of these oxides as NaCl sensors. The single phase materials of NiO, CuO, Fe_2O_3 and Co_3O_4 were synthesized using evaporation method employing NaCl template. Figure 4.1 is showing the schematic drawing for the formation of hollow cubic material. The general route for production of NaCl templated porous transition metal oxides includes following steps,

- Impreging of NaCl into the metal solution.
- Metal oxide clusters formation outside the NaCl.
- Crystal growth by annealing.
- Removal of NaCl template.
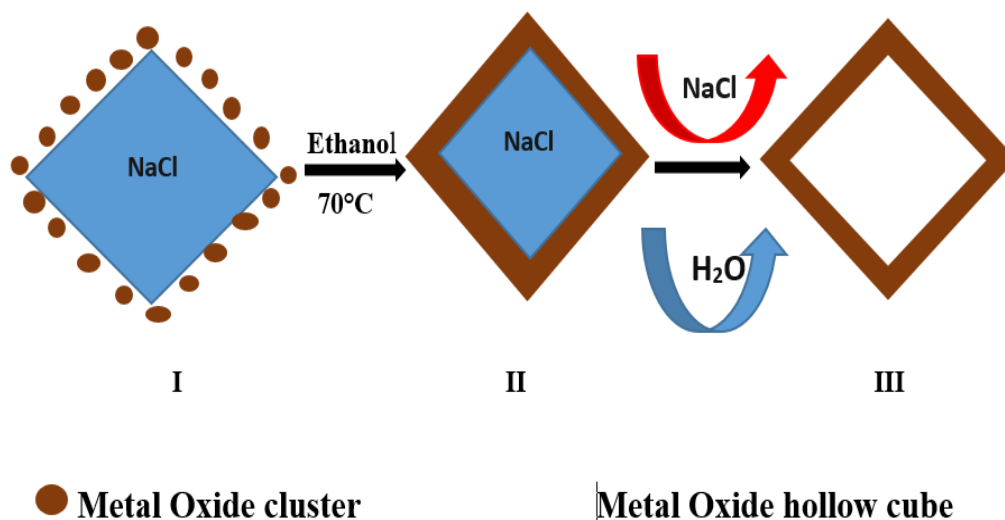
Figure 4.1. Showing the formation of templated mesoporous oxide

Obviously the most important step is the impregnation of the template. Until now, there are four methods reported on successful impregnation of templates into the metal containing precursors; i. Evaporation method, ii. Surface modification method, iii. One-step nanocasting method and iv. Dual solvent method. The most popular one out of these is the evaporation method in which the template is combined with selected precursor salt in ethanol. The template is generally accepted to migrate into the

precursor by capillary action during the evaporation of ethanol. But it was found that the impregnation process of a template might not take place during the evaporation but mainly occurred during annealing after the evaporation [36]. The NaCl template was impregnated into the metal precursor solutions which caused the growth of metal oxide outside the sodium chloride and then porous product is finally obtained by the removal of central template. Therefore some factors including the selection of metal precursors, selection of template, impregnation method and removal of template are crucial to such synthesis. Non-covalent imprinting sounds to influence more capability for the future of imprinting owing to extensive and enormous compounds inclusive biological, which are competent for non-covalent interactions with a metal oxides.

4.1   X-ray Powder Diffraction (XRPD)

The XRPD patterns of NiO, CuO, Fe_2O_3 and Co_3O_4 as shown in figures 4.1a-d show that the materials are a single phase. All the XRPD patterns of NiO, CuO, Fe_2O_3 and Co_3O_4 confirmed the purity of metal oxides and clearly showed the template (NaCl) was completely detached from as-synthesized metal oxides. It can be observed that non-imprinted metal oxides exhibit better crystalline than imprinted templated metal oxides, indicating that the latter is composed of far smaller crystalline grains. This is ascribed to that solid NaCl salts remained in the mesospheres prevented the metal oxides grains from growing to larger size in the evaporation process.
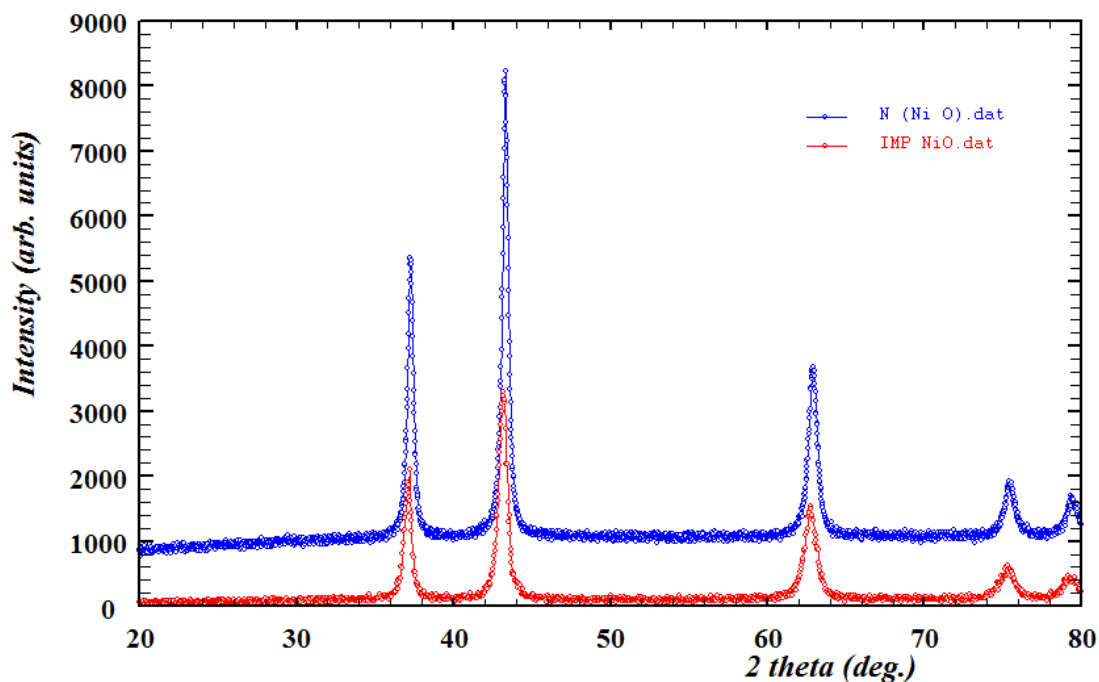
Figure 4.1a XRPD pattern of NiO

In Figure 4.1a. XRPD pattern of NiO, peaks are indexed to Cubic geometry space group $Fm3m$ (no.166) with lattice constants, a =2.95749(6), c = 7.255(4) Å.
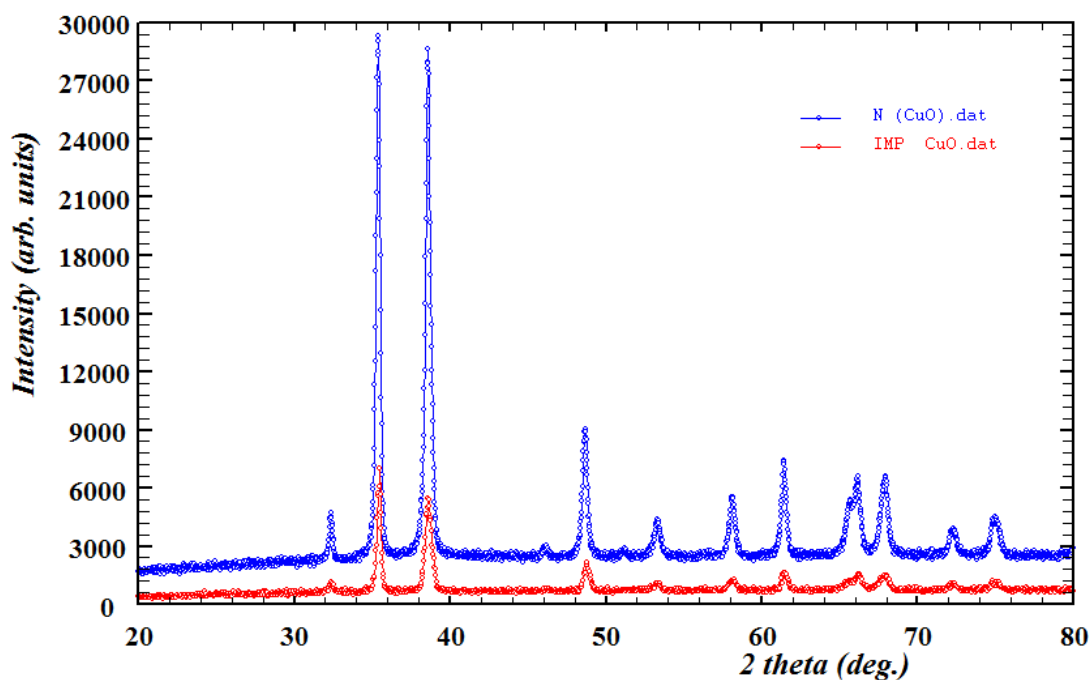

Figure 4.1b XRPD pattern of CuO

In Figure 4.1b. XRPD diffraction pattern of CuO is indexed to monoclinic symmetry C_2/c (no. 15) with lattice constants, a =4.6797, b =3.4314, c = 5.1362 Å and β=99.262º.
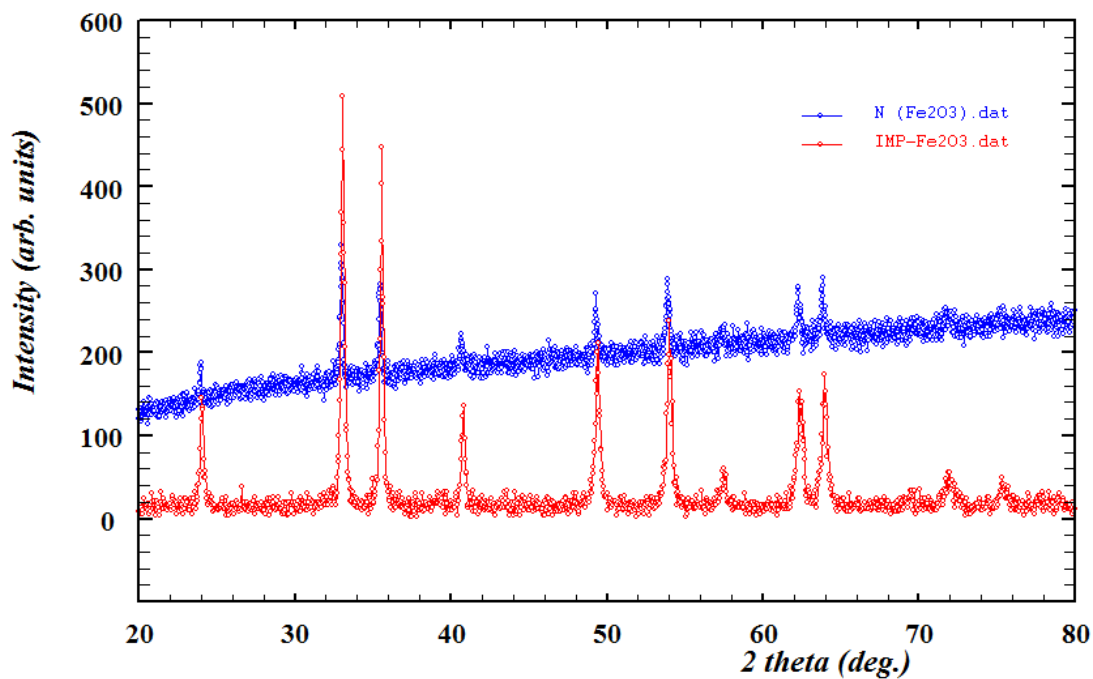
Figure 4.1c XRPD pattern of Fe₂O₃

In Figure 4.1c. XRPD pattern of Fe_2O_3 is indexed to Rhombohedral symmetry in space group $R\bar{3}$ (no.148) with lattice constants, a =5.0380, b =5.0380, c = 13.7720 Å.
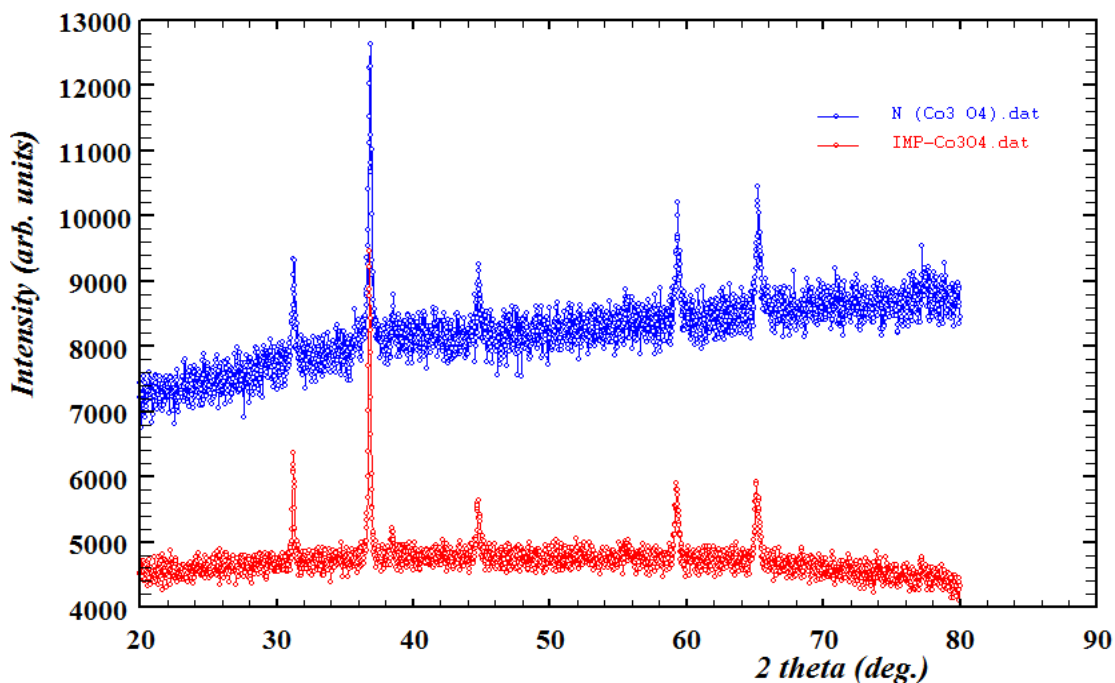

Figure 4.1d XRPD pattern of Co₃O₄

In Figure 4.1d. XRPD pattern of Co_3O_4, peaks are indexed to cubic with space group Fd3m (no.227) along with lattice constants, a =8.0968, b =8.0968, c = 8.0968 Å.

4.2 SEM

The qualitative analysis and morphology of the samples were determined by SEM. The difference in the particle and crystallite size is due to crystalline agglomeration. Figure 4.2a shows the SEM image of NiO depicting average particle size as 102 nm. The particles were highly agglomerated yet clear cubic morphology was obvious. Figure 4.2b shows the SEM images of CuO with irregular hexagonal morphology and particle size range of 124 nm. CuO particles are less agglomerated and more defined and as compared to NiO. Figure 4.2c shows SEM image of Fe_2O_3 distorted cubic particles with size range of 341 to 356nm ($\sim$0.356μm) and rough surface after removal of template. The particle size of $NaNO_3$ templated Fe_2O_3 were 0.2-1.8μm [95]. The Co_3O_4 particles were of 250-300nm ($\sim$0.25-0.30μm) size with a very regular octahedron morphology is showing in figure 4.3d. The NaCl templated Co_3O_4 with 1-2μm particle size and octahedron morphology has been reported already [59]. Due to different crystal structure these templated metal oxides showed different morphologies. Another phenomenon was observed that the crystal symmetry played a crucial aspect all along the crystal growth. Co_3O_4 and NiO is found to have a cubic structure, while the other tested oxides i.e. CuO (monoclinic), and Fe_2O_3 (rhombohedral). Non-cubic metal oxides might not be imitated outside NaCl using evaporation method. Definitely, saturation of the template for non-cubic oxides motives no appropriate obstacles and complications. It is expected, that in the interim of crystal growth outside template, there is a momentous cooperation betwixt crystals and walls of NaCl. Cubic oxides may developing isotropically, stuffing cubic template walls perfectly from outside. Withal, non-cubic oxide crystals grow and interact with the NaCl walls anisotropically, culminating in preponderant distortion of the structure.

Figure 4.2 SEM images of non-imprinted metal oxides a) NiO b) CuO c) Fe_2O_3 d) Co_3O_4 .It was found that non-imprinted metal oxides have smaller particle size as compared to templated metal oxides. The particle size of non-imprinted NiO, CuO, Fe_2O_3 and Co_3O_4 is 46, 54, 78 and 66nm respectively. Figure 4.4 is showing the impregnation of NaCl inside the metal oxides.
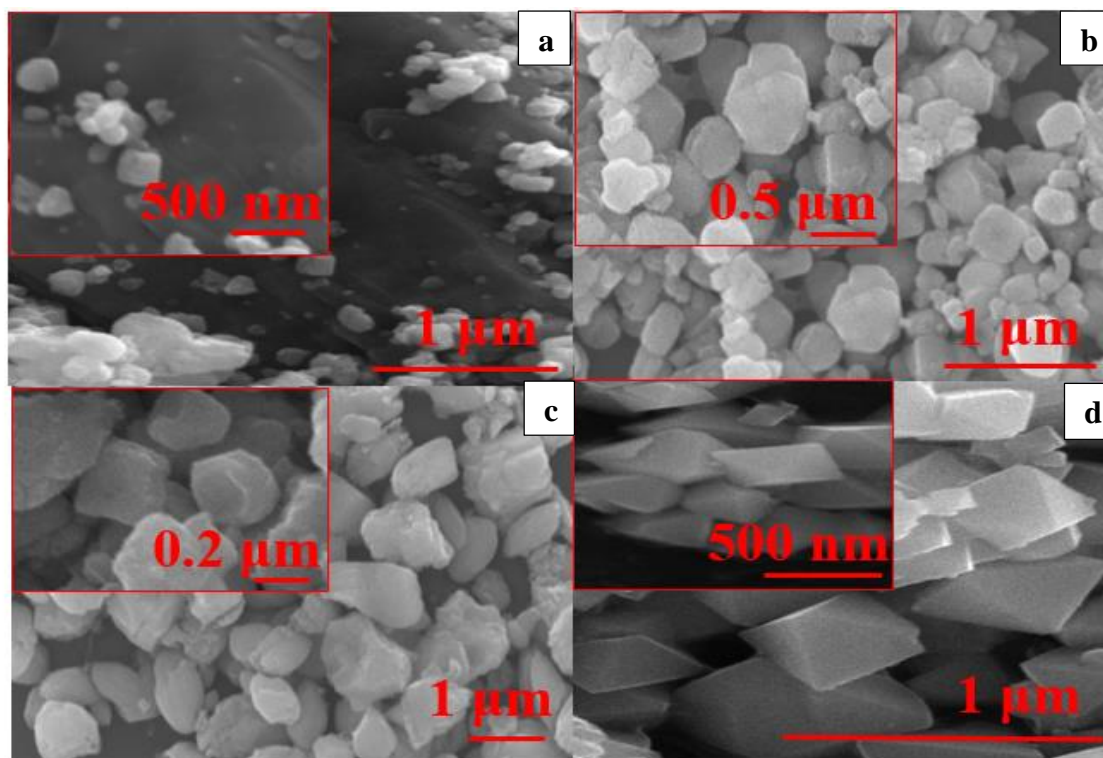
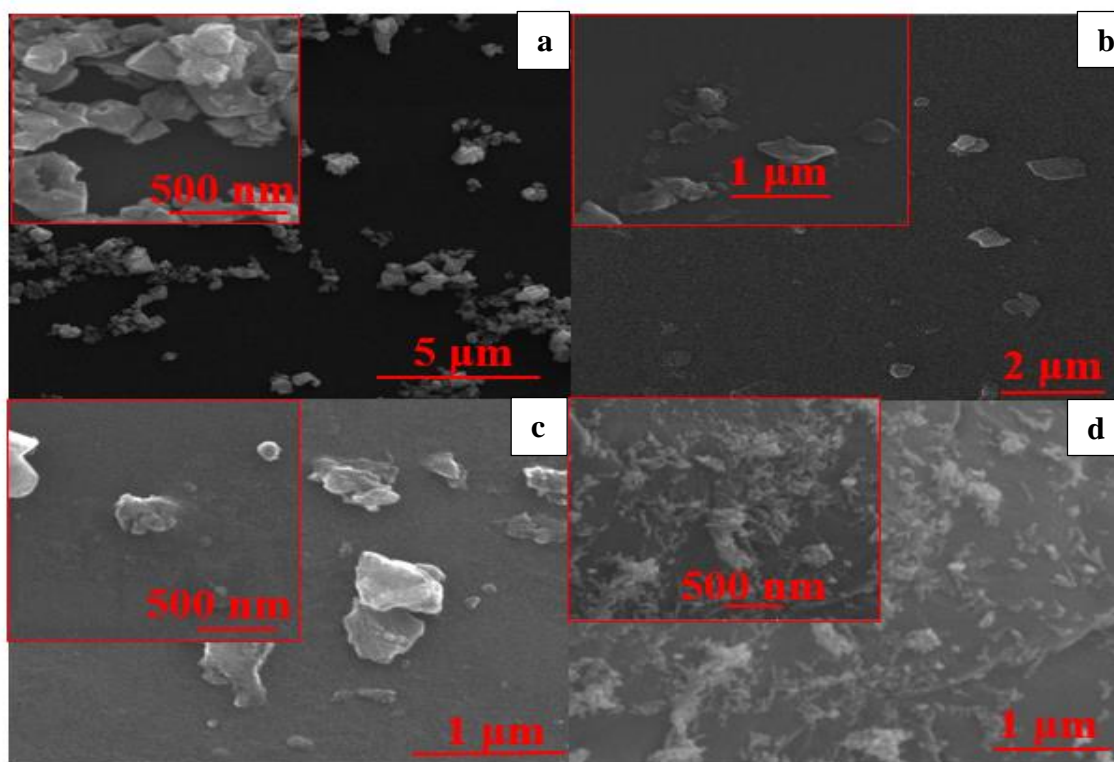*Figure 4.2. SEM images of Imprinted oxides a) NiO b)CuO c) Fe₂O₃ d)Co₃O₄*

Figure 4.3. SEM images of non-imprinted oxides a) NiO b) CuO c) Fe₂O₃ d) Co₃O₄
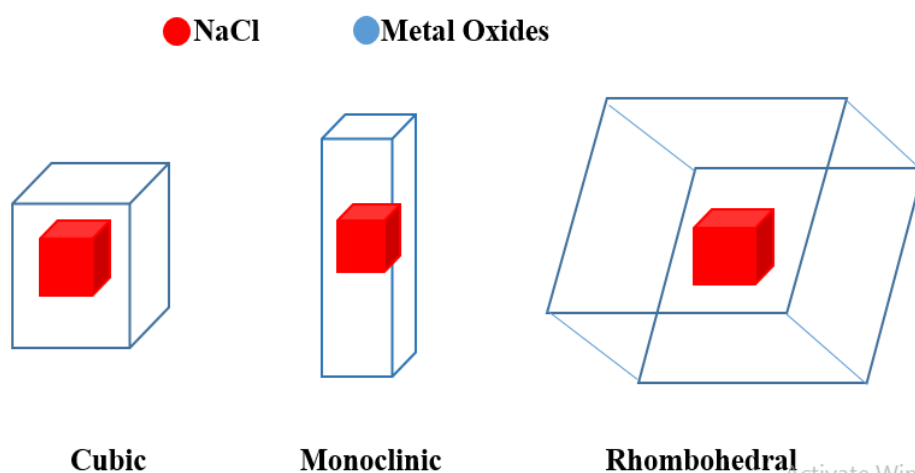
Figure 4.4. showing the impregnation of NaCl inside the metal oxides

4.3 AFM

AFM was used for quantitative roughness measurements and imaging the surface morphology. Figure 4.5 a-d are showing the 3D image of NiO, CuO, Fe_2O_3 and Co_3O_4 with the surface roughness of 89.7nm, 8.80, 3.52 and 25.5nm, respectively. All templated metal oxides exhibited good surface roughness, which is a clear indication of complete removal of template the NaCl, leaving the porous and rough structure. More roughness is achieved by NiO owing to its small particle size along with more surface area. Lower roughness is exhibited by CuO and Fe_2O_3 showing that they are less porous as compared to Cubic NiO and Co_3O_4.The 25.5 nm roughness of cubic Co_3O_4 is lower than cubic NiO indicating that it has porous or rough structure due to its large size.
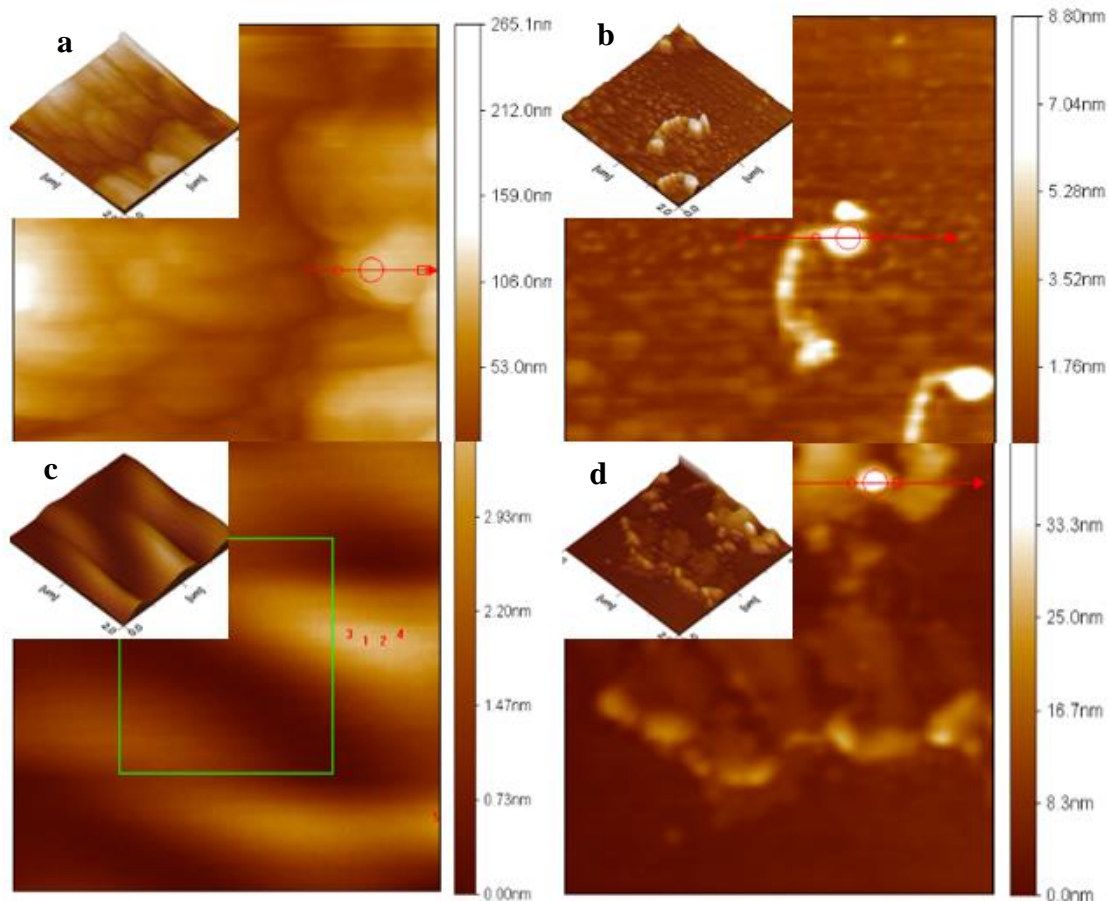
Figure 4.5. AFM images a.NiO, b. CuO, c.Fe₂O₃, d. Co₃O₄

4.4   Nitrogen Adsorption

The Nitrogen adsorption isotherm and the pore size distribution of four samples are profiled in Figs. 4.6 and 4.7.

a. *BET*. All of them exhibit typical IV isotherm with the hysteresis loop, illustrating the mesoporous structure of templated metal oxides. As shown in figure 4.6a) NiO 4.6b) CuO 4.6c) Fe_2O_3 4.6d) Co_3O_4.
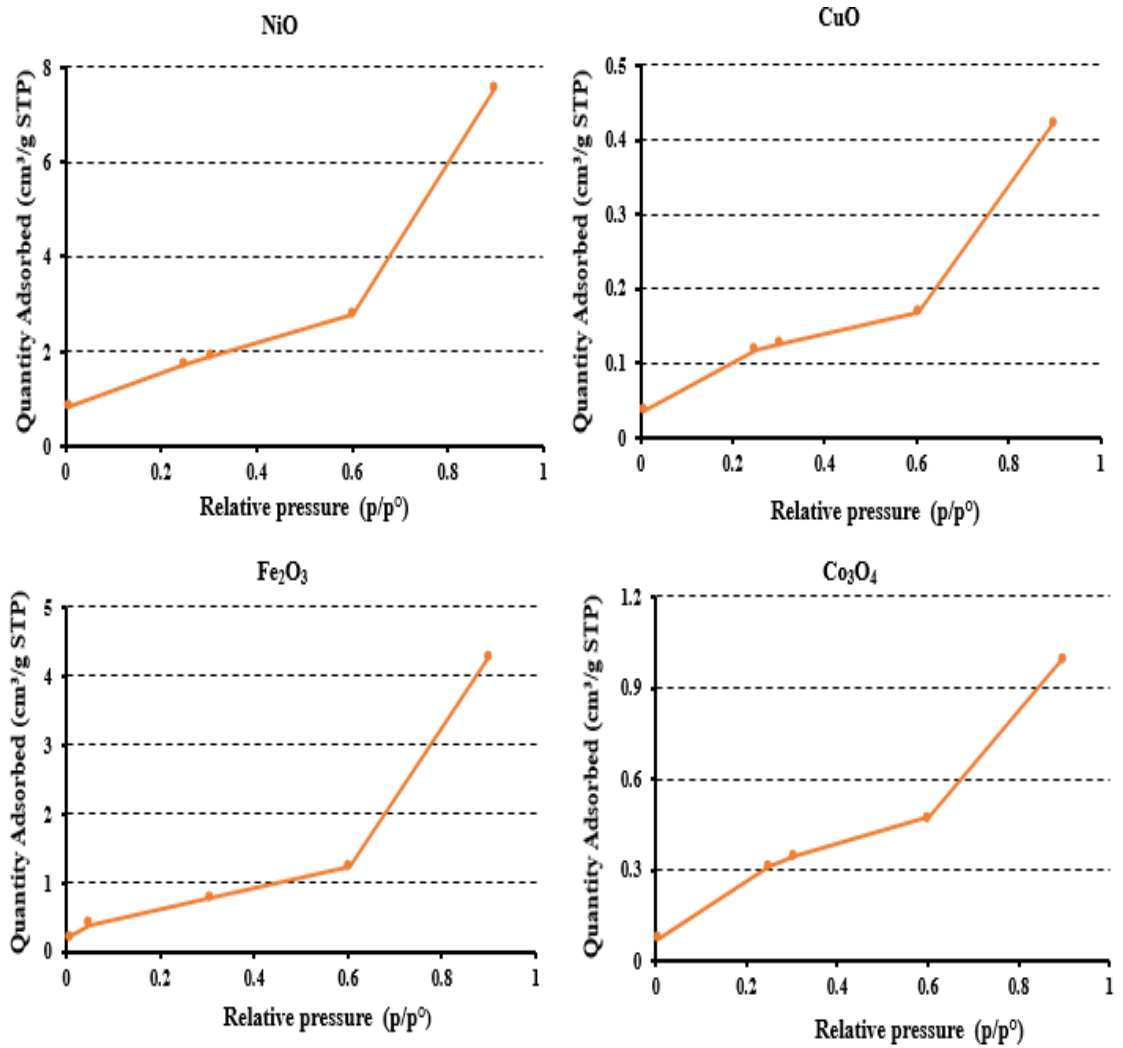
Figure 4.6. Adsorption isotherm of TMOs.

b. DFT. Density functional theory pore size distribution of mesoporous metal oxides were achieved established on the N_2 isotherms borne out at 77 K. And the average pore size displayed distinct increment, ranged from 5 to 15 nm. The pore volume remains constant from 0 to 5 nm. The maximum pore volume is achieved by NiO as shown in figure 4.7a. The maximum pore volume 0.0109 cm^3/g at the pore size of 15.9 nm is due to the smallest particle or crystallite size. The CuO has the pore volume of 0.000623 cm^3/g as showing in figure 4.7b. Figure 4.7c is showing that Fe_2O_3 has the pore volume of 0.00614 cm^3/g. Figure 4.7d illustrates that cobalt oxide achieved 0.00146 cm^3/g pore volume at the maximum of 15.9 nm pore size. 15.9 nm is the maximum pore size achieved by all metal oxides showing that all metal oxides are in range of mesoporous materials and being Templated.
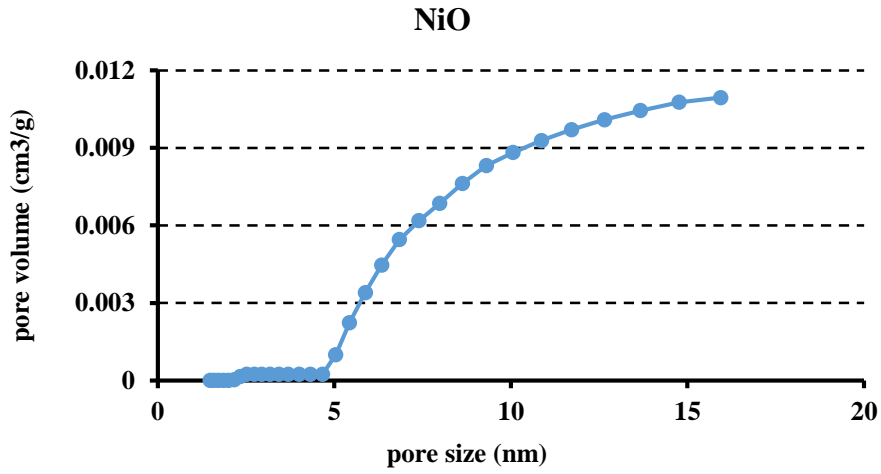
Figure 4.7a DFT pore size distribution of NiO
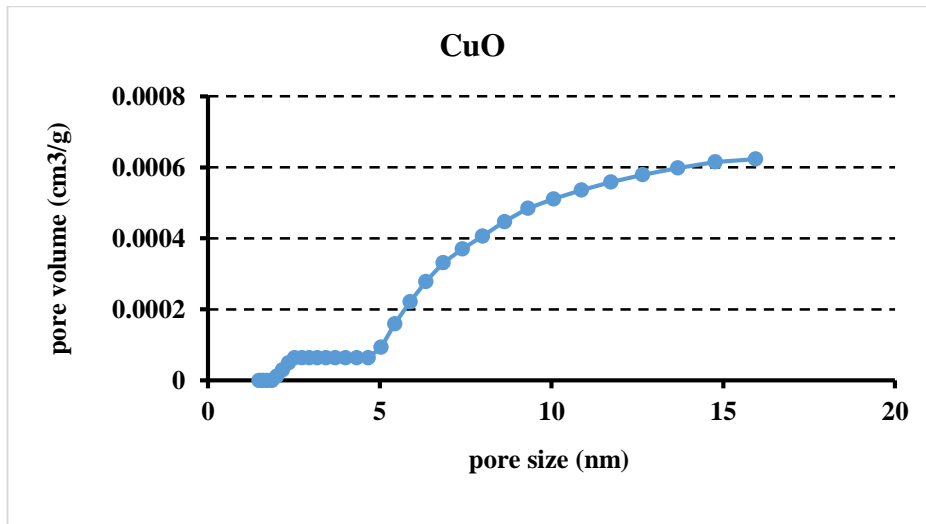
Figure 4.7b DFT pore size distribution of CuO
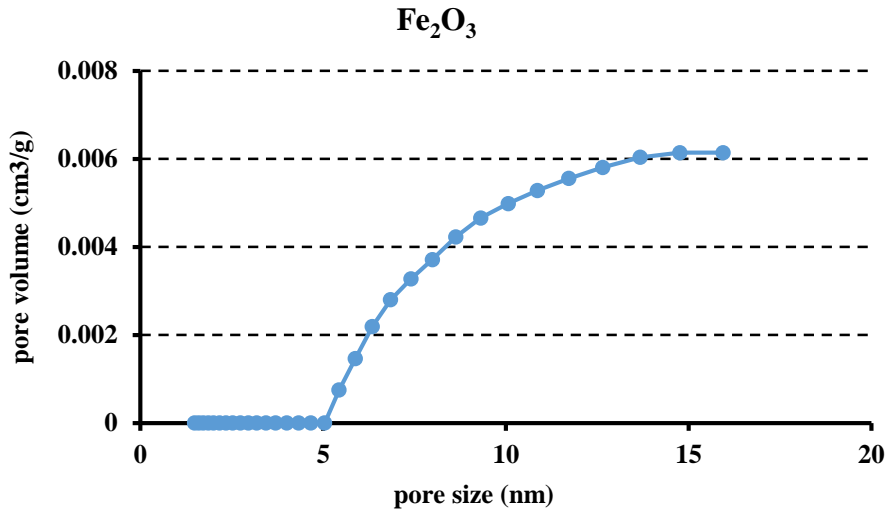
Fe₂O₃

Figure 4.7c DFT pore size distribution of Fe₂O₃

Co₃O₄

Figure 4.7d DFT pore size distribution of Co₃O₄

Table 4.1 Different parameters of templated and non-templated metal Oxides

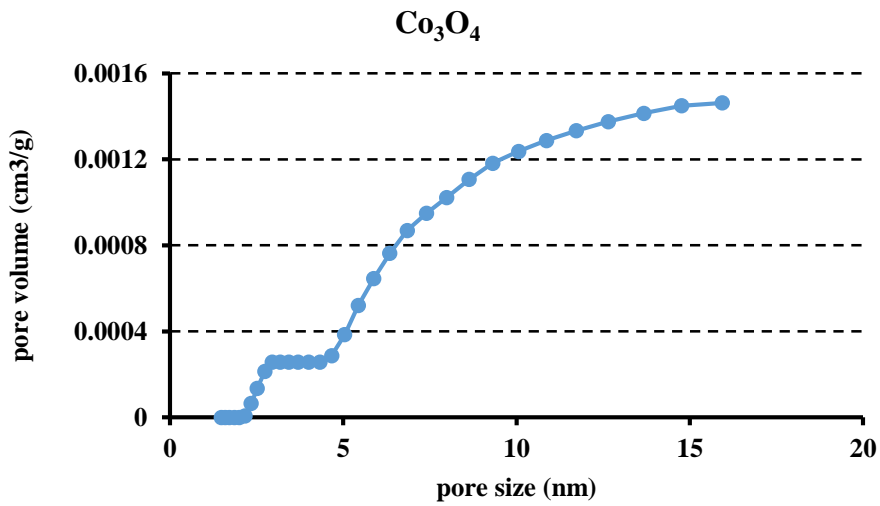| Parameters	NiO	CuO	Fe$_2$O$_3$	Co$_3$O$_4$
crystal structure	Cubic	Monoclinic	Rhombohedral	Cubic
Space group	Fm3m	C2/c	$R\bar{3}$	Fd3m
Crystallite size (nm) of imprinted oxides	32.23	37.63	52.27	153.88
Crystallite size (nm) of non-imprinted oxides	49.72	71.03	134.44	203.06
Morphology	cubic	hexagonal	cubic	Octahedron
Particle size (nm) of Imprinted metal oxides	102	124	341-356	250-300
Particle size (nm) of non-imprinted metal oxides	46	54	78	66
Surface roughness (nm)	89.7	8.8	3.5	25.5
BET max N$_2$ adsorption (cm^3/g)	7.6	0.4	4.2	0.9
DFT avg pore volume (cm^3/g)	0.0036	0.0002	0.0019	0.0006
DFT avg pore size (nm)	6.16	5.97	6.16	6.16
Saline Sensing (nF)	5.4	5.1	7.1	6.1

4.5   Sensor characteristics

The work nonce the employment along with advancement of low-cost salinity sensing Sodium chloride is contemplated as essential content for testing owing to its extrusive abundance in water bodies Sensor was defined by trialing diverse concentrations of NaCl. Now, a lot of research work is enduring to resolve the ideal concentration of salinity in sea. It is pricey to clear away the surplus salt from sea water owed to the tremendous-quality machinery desired to excerpt salt but it can be sensed.

4.5.1 Functioning Principle of Sensor

Electrodes over sensor spots were arranged in an interdigitated pattern. Sensor area operates by capacitive mechanism, where one electrode is treated as the reference electrode and other excitation one at which the voltage was supplied. Time-reliant voltage signal is catered to the excitation one, after which an electric field is developed betwixt conversely charged electrodes. Field distended betwixt them owed to their flat framework. Single directional measurement plight was arranged owed to an insulating material to the electrodes. Field brinks over each material in proximity to sensor. Aforementioned alters properties of an area which is utilized to regulate the aspects of certified material. Ingress extent of the electric field is changed by changing the spatial wavelength (distance betwixt electrode fingers of identical polarity), that creates it an attractive prime for scientific along with industrial purposes.

Due to pretreatment/specimen preparation or frequently tiresome affair, it is eminently alluring to establish a sensor scheme which is uncomplicated, profitable, robust and applicable as actual-time calibrations. Utmost of published papers about molecular ion imprinting accord by synthesis or characterization of imprinted resins/polymers. Lately novel field has been popularized within the area of imprinting, in which corresponding products as receptor films are enforced over sensitive electrodes. The aim of present research is to generate a direct, smooth and tag free sensor by imprinting for espial of sodium chloride ion in solution. For that intention we used templated metal oxides as a sensing material.

The experiments were performed with a JET-7600 plus precision LCR meter at a frequency of 1000 HZ. Metal oxide films were utilized as a basic material to establish sensor. A suspension of 3 mg powder sample was made in 300 μL DI water by sonicating it for 20 min. Later on a thin film of suspension was applied on the interdigital electrode by drop-coating method. This electrode was then dried completely by keeping at 100°C for 20 min. NaCl was utilized as solute to make solutions for salinity check. DI MilliQ® water (Resistance: 17.2 MΩcm or pH: 6.82) was utilized as solvent for the analysis. Sequential dilution were achieved to make a set of solutions from 50ppm to 5ppm. Electrochemical sensing was carried out to resolve sensor behavior during examining upon distinct salt concentrations. This instrument can accommodate samples up to 8″ in diameter. and 12mm thick in air, vacuum, or fluids. Solution capacitance, impedance and resistance are the

specifications that influences kinetic sensor response which may rely upon the assets of medium. When solution medium is replaced, conductivity of sensor or relative permittivity (εr) also alters .This leads to change in the resistance and capacitance of the solution. The capacitance and conductance increases by increasing the concentration of the Analyte, whereas resistance decreases by increasing concentration. Coating templated metal oxide on interdigitated electrode gives detectable sensor responses relying on the content of sodium chloride solutions. Besides, sensor response from 5 ppm to 50 ppm concentration demonstrates fully reversible along with linear or definite sensor signals. Evidently, sensor characteristic is linear with excellent correlation ($R^2 > 0.95$) within the concentration range 0 to 50 ppm. Figure 4.8 is showing the scheme of sensing measurements.
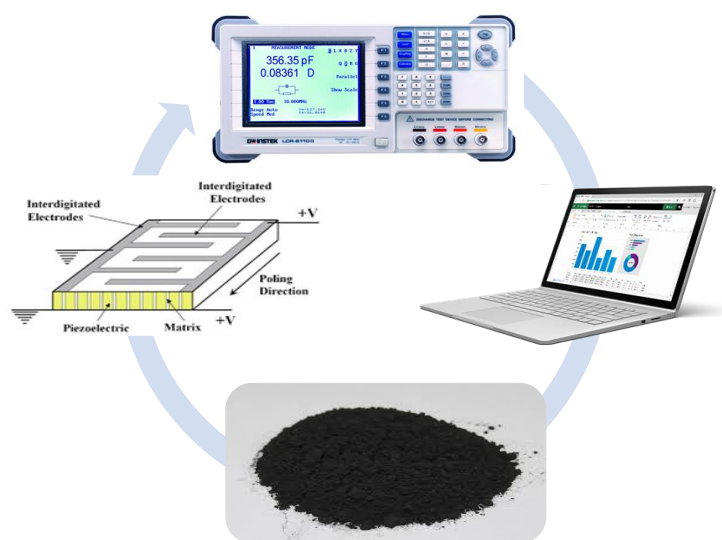

Figure 4.8. is showing the scheme of sensing measurement

Figure 4.9a and 4.9b shows the sensitivity response of NiO with a limit of detection 0.72 ppm. The sensor response is linear with concentration. The sensor response increases with the increase in concentration of sodium chloride solution from 0 to 50 ppm. In NiO the R^2 value is 0.9566. Figure 4.10a is showing that sensor response is also reversible. Figure 4.10a and 4.10b is showing the sensitivity graphs of CuO with a limit of detection 0.44 ppm. The R^2 value is 0.9666 with reversible sensor response. Graphs of Fe_2O_3 are shown in figure 4.11a and 4.11b. The maximum value of $R^2 = 0.9754$ is achieved by Fe_2O_3 with good sensitivity and 0.20 ppm limit of detection along with reversibility as shown in time graph of 4.511b. Figure 4.12a and 4.12b are showing the graphs of Co_3O_4 with $R^2 = 0.9664$ and reversible sensor response with a 0.21 ppm limit of detection. The maximum sensitivity and selectivity is achieved by

Fe_2O_3 is due to its ions in which Fe^{+3} is the hard acid and O^{-2} is the hard base makes good coordination with sodium chloride in which Na^{+1} is the hard acid and Cl^{-1} is the hard base. In NiO and CuO the Ni^{+2} and Cu^{+2} are the border line acids, whereas in Co_3O_4 the Co ion exists in two oxidation states +2 and+3, in which Co^{+3} is the hard acid which makes it good sensor for sodium chloride solution and Co^{+2} is the border line acid which decreases its sensitivity as compared to Fe_2O_3.
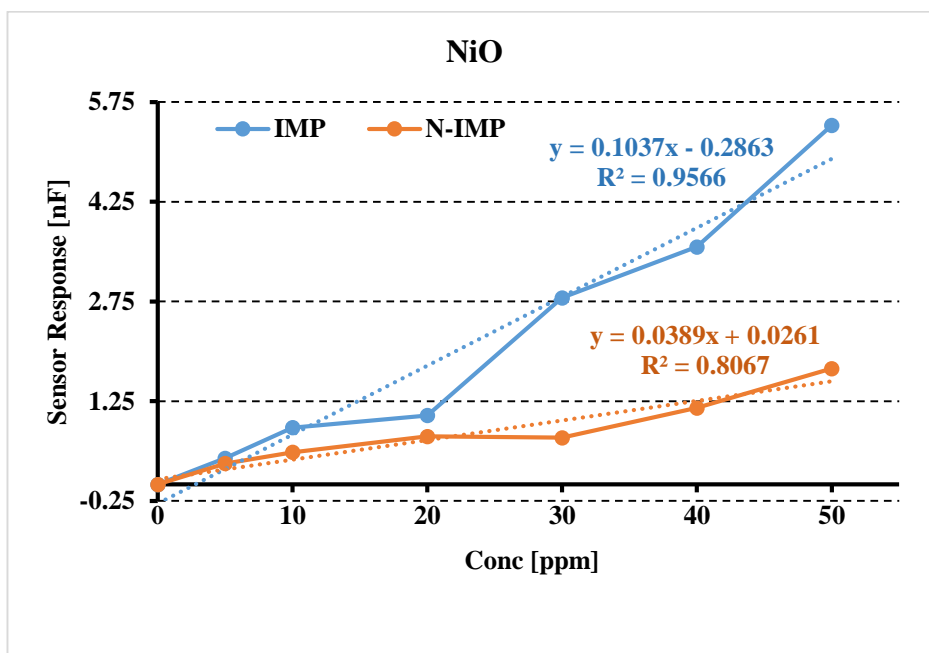
Figure 4.9a sensor Response of NiO
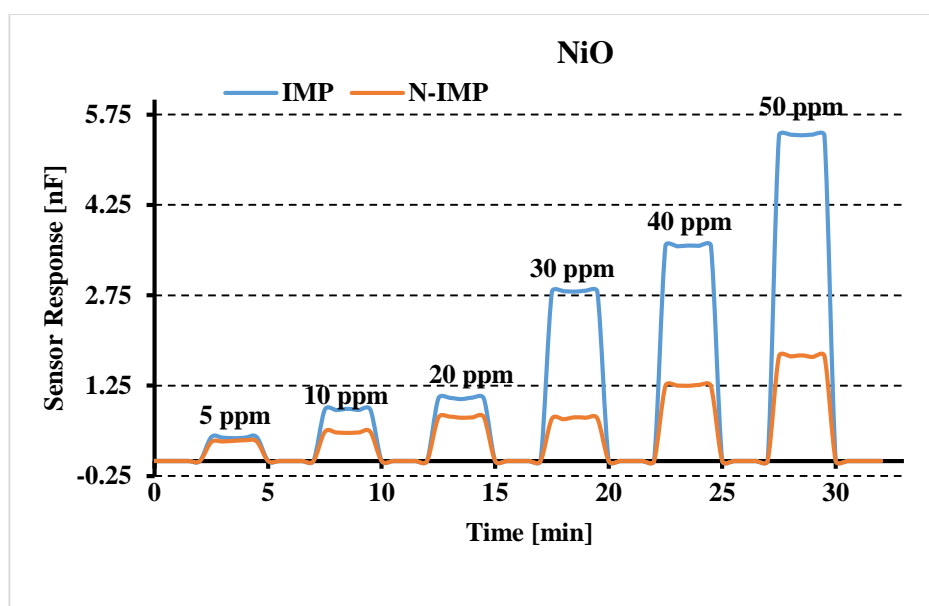
Figure 4.9b Time graph of NiO
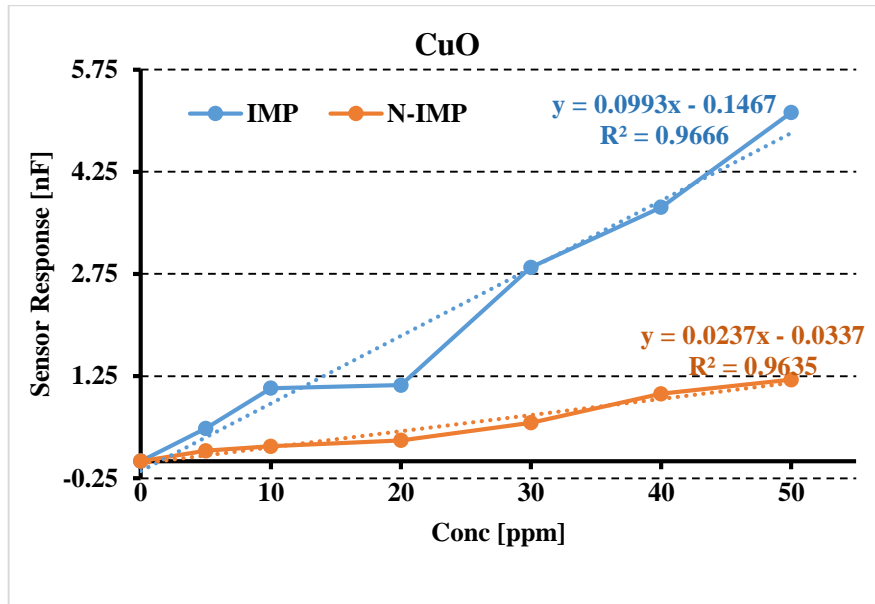
Figure 4.10a sensor Response of CuO
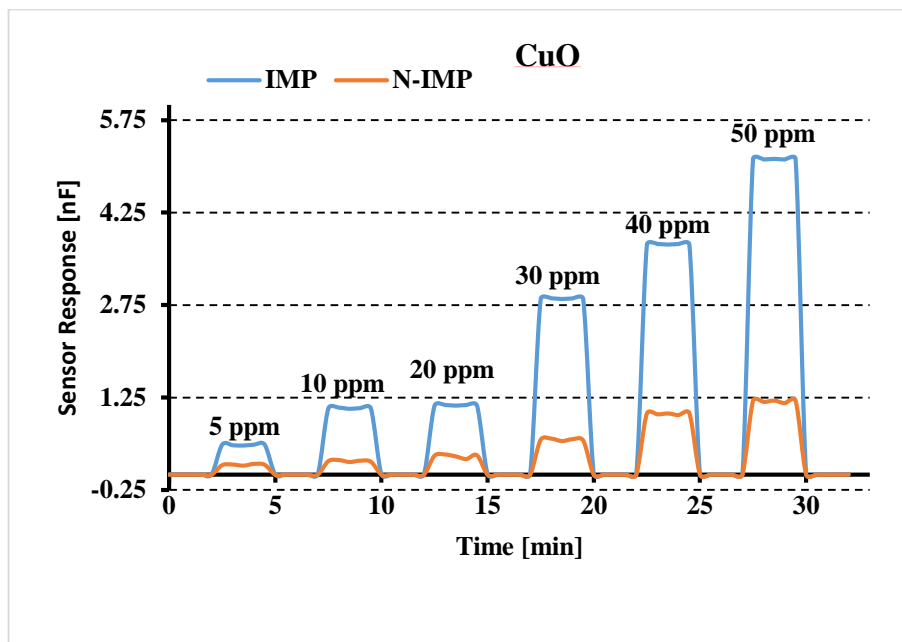
Figure 4.10b sensor Response of CuO
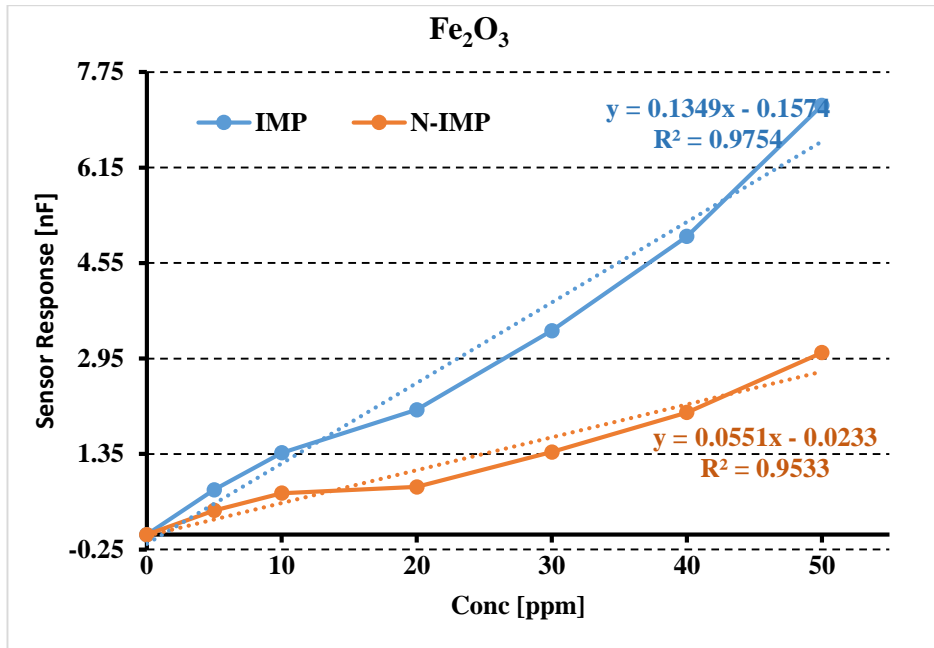
Figure 4.11a Sensor Response of Fe_2O_3
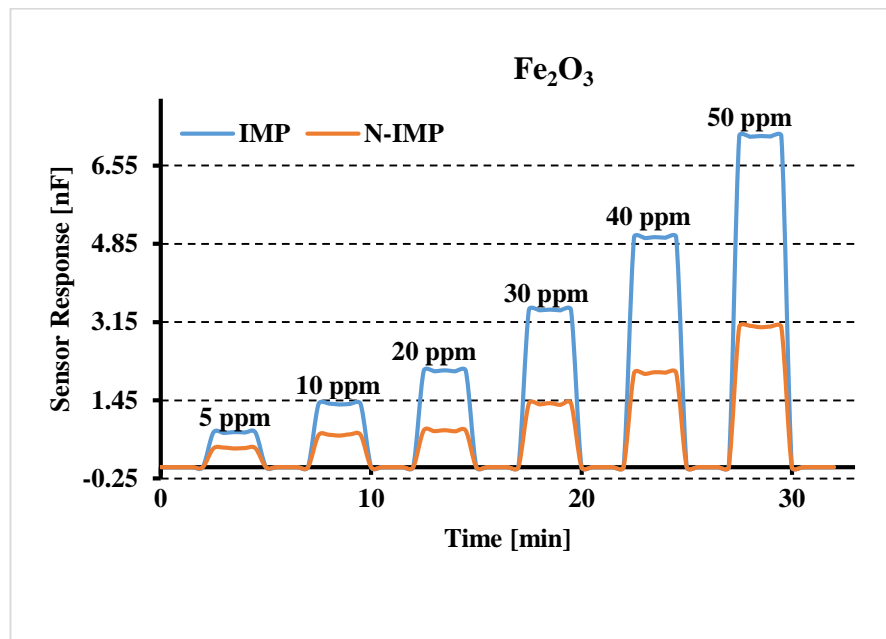
Figure 4.11b Time graph of Fe_2O_3
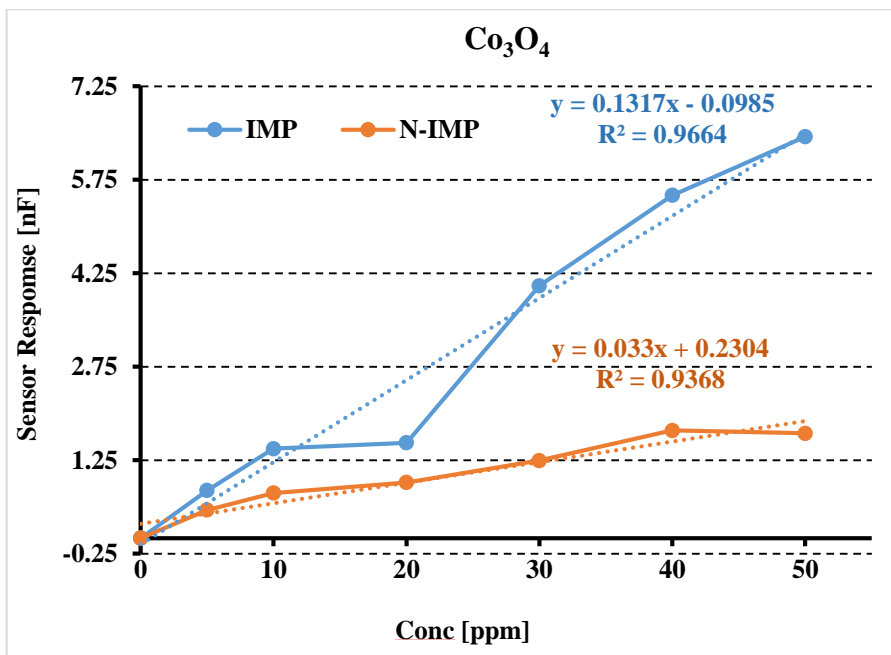
Figure 4.12a Sensor Response of Co₃O₄
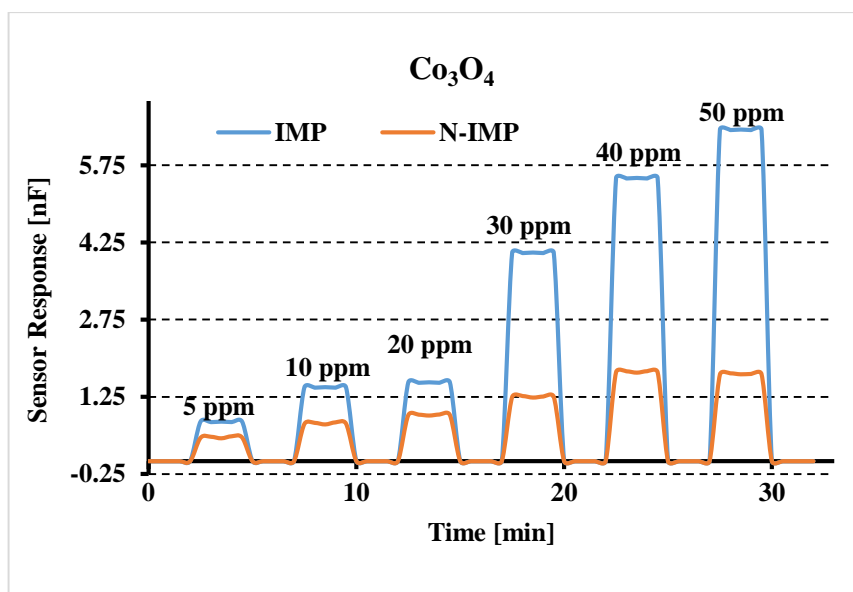
Figure 4.12b Time graph of Co₃O₄

4.5.2 Selectivity

To check the selectivity of mesoporous transition metal oxides 50 ppm solutions of NaCl, $CaCl_2$, KCl, NaF and KBr were prepared in DI water. If ion imprinting is certainly positioned on coordination, the culminating cavities are resolving by the non-covalent interaction forming strength of template relative than geometry. Figures 4.13a, b, c and d. outlines selectivity feedback of NaCl imprinted metal oxides for the following salts NaCl, $CaCl_2$, KCl, NaF and KBr. Apparently, sensor feedback is 3.6

stages greater for NaCl than for any of the alternative salt. All the templated metal oxides are selective towards the sodium chloride. The better selectivity of metal oxides towards NaCl is due to the same ionic radius and cavities formed by NaCl as compared to other salts in metal oxides. Besides, it is observed that the cavities developed for NaCl are not only responsive to the size of contending ions though likewise to their oxidation states. In NaCl the Na^{+1} has the ionic radius of 116 pm and Cl^{-1} has the ionic radius of 167pm, while it is different in other salts. Table 4.1 summarizes the ionic radius of different salts. By changing the salts the anionic and cationic radius changes, which decreases the binding of other salts towards metal oxides as compared to NaCl. So, metal oxides showed better selectivity towards sodium chloride.

Table 4.2 Selectivity Response of templated metal Oxides towards different salts

Salts	Cationic radius (pm)	Anionic radius (pm)
NaCl	116	167
$CaCl_2$	114	167
KCl	152	167
NaF	116	119
KBr	152	182

NiO

Figure 4.13a Selectivity Response of NiO

CuO
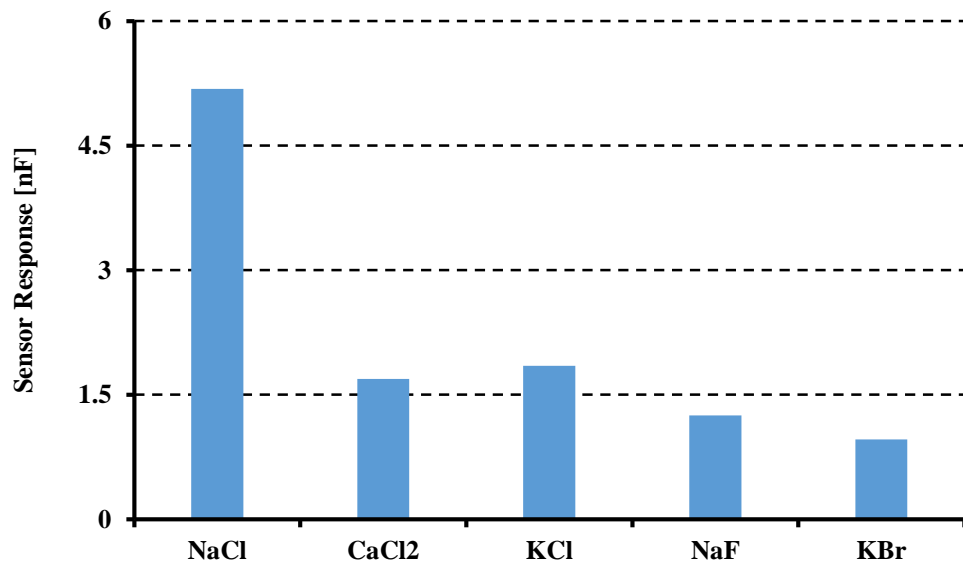
Figure 4.13b Selectivity Response of CuO
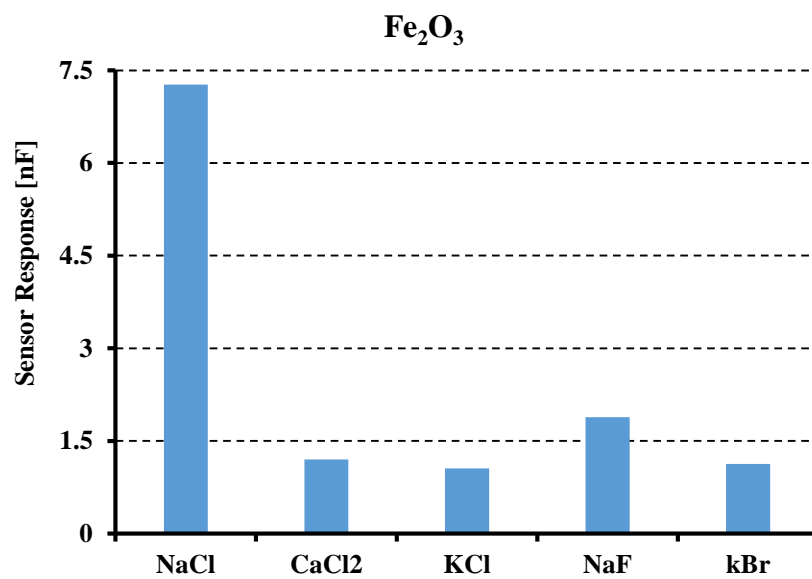
Fe₂O₃

Figure 4.13c Selectivity Response of Fe₂O₃
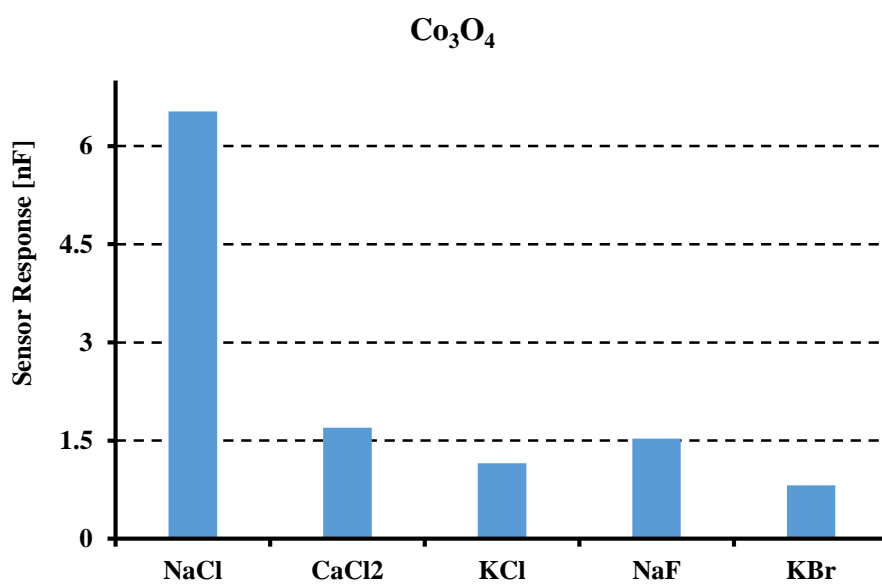
Co₃O₄

Figure 4.13d Selectivity Response of Co₃O₄

4.6 Conclusions

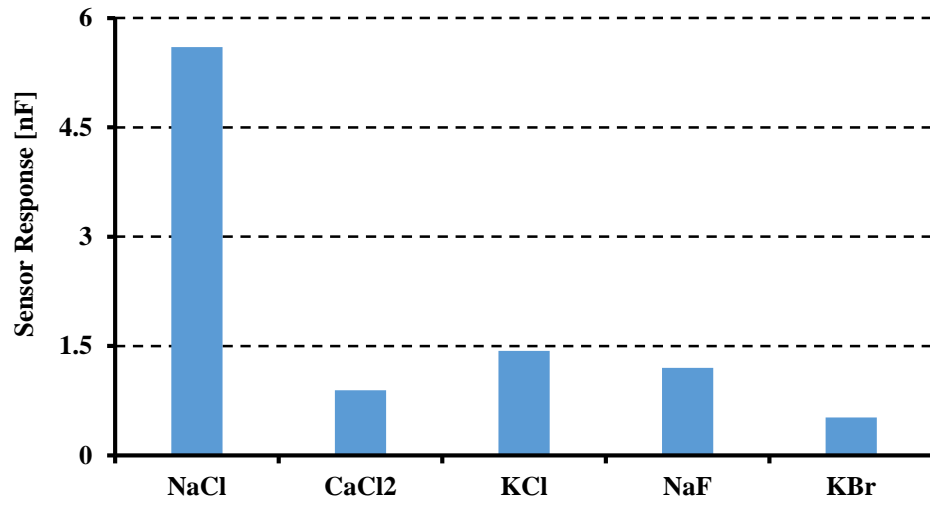Molecular Imprinting Technology, often expressed as a method of accomplishing a molecular lock to match a molecular key, is a technique for the formulation of molecularly imprinted materials with tailor-made binding sites correspondent to the template molecules in shape, functional group or size. Porous metal oxides, NiO, CuO, Fe_2O_3 and Co_3O_4 have been synthesized by using NaCl template. The NaCl template then transformed into the metal oxide core by capillary action. The metal oxides were formed and grew outside the NaCl template. Single crystals of porous NiO, CuO, Fe_2O_3 and Co_3O_4 were proven to be synthesized successfully after the washing of NaCl core, characterized by XRPD, SEM, AFM and Nitrogen adsorption technique etc. The response of synthesized materials as sensor was analyzed by LCR meter at different NaCl concentrations. Whereas, selectivity of the templated metal oxides was best for NaCl as compared to KCl, $CaCl_2$, NaF and KBr.

4.7 Future Prospects

Some novel metal oxides such as ZrO_2 which was not prepared will be investigated to be synthesized using NaCl template. Once the novel porous metal oxides are synthesized, their properties will be examined such as the catalytic activity, energy storage and solid state electrochemical properties. Additionally, the Cyclic Voltammetry technique will be applied to check the energy storage capacity of porous materials in Batteries Fuel cells and drug delivery. The sensitivity of these porous metal oxide will be monitored by using different salts and template to sense toxic elements in polluted water and air. The non-imprinted inorganic materials will also be synthesized to compare the properties and sensitivity with imprint mesoporous metal oxides.

References

[1]   M.Helene , "Elaboration of a new sensor based on molecularly imprinted polymers for the detection of molecules in physiological fluids ," 2014.

[2]   K. Kotova, M. Hussain, G. Mustafa, and P. A. Lieberzeit, "MIP sensors on the way to biotech applications.," *Sensors Actuators, B Chem.*, vol. 189, pp. 199–202, 2013.

[3]   E. Yılmaz, B. Garipcan, H. K. Patra, and L. Uzun, "Molecular imprinting applications in forensic science," *Sensors (Switzerland)*, vol. 17, no. 4, pp. 1–24, 2017.

[4]   S. Lingxin, "Molecular imprinting : perspectives and applications," *Chem. Soc. Rev.*, vol. 45, pp. 2137–2211, 2016.

[5]   M. J. Whitcombe, N. Kirsch, and I. A. Nicholls, "Molecular imprinting science and technology: A survey of the literature for the years 2004-2011", vol. 27, no. 6. 2014.

[6]   I. Muhammad, I. Naseer, M.Adnan, A. Adeel, H. Tajamal, S.Ahsan, A.Ejaz and M.A. Muhammad,"Molecularly Imprinted Nanomaterials for Sensor Applications," *Nanomaterials*, vol. 3, no. 4, pp. 615–637, 2013.

[7]   A.Cameron, S.A. Hakan, I.A. Lars, J.A. Richard , K.Nicole, A.N. Ian, O. John and J.W. Michael , "Molecular imprinting science and technology: A survey of the literature for the years up to and including 2003," *J. Mol. Recognit.*, vol. 19, no. 2, pp. 106–180, 2006.

[8]   H. Yan and K. Ho Row, "Characteristic and Synthetic Approach of MolecularlyImprinted Polymer," *Int. J. Mol. Sci*, vol. 7, pp. 155–178, 2006.

[9]   N. Pal and A. Bhaumik, "Soft templating strategies for the synthesis of mesoporous materials: Inorganic, organic-inorganic hybrid and purely organic solids," *Adv. Colloid Interface Sci.*, vol. 189–190, pp. 21–41, 2013.

[10]   M.Adnan, A.L Peter and L.D. Franz ," Chemical Sensors Based on Molecularly Imprinted Sol-Gel Materials _ HTML." *Materials.,* vol.3, no. 4, pp. 2196-2217, 2010.

[11]   C. Dong , R. Lu, Z. Huaizhou, X. Chenjia, Z. Lu , Y. Ying, W. Hengzhi, L.Yucheng , F.R Mary , H.C Jeffrey, J.N Michael, R. Zhifeng and C.C Thomas, "A molecular-imprint nanosensor for ultrasensitive detection of proteins," *Nat. Nanotechnol.*, vol. 5, no. 8, pp. 597–601, 2010.

[12]   I. I. Slowing, B. G. Trewyn, S. Giri, and V. S. Y. Lin, "Mesoporous silica nanoparticles for drug delivery and biosensing applications," *Adv. Funct. Mater.*, vol. 17, no. 8, pp. 1225–1236, 2007.

[13]   M.Klaus, "The Promises of Molecular Imprinting," 2006.

[14]   P. S. Sharma, F. D'Souza, and W. Kutner, "Molecular imprinting for selective chemical sensing of hazardous compounds and drugs of abuse," *TrAC - Trends Anal. Chem.*, vol. 34, pp. 59–76, 2012.

[15] K. Haupt and K. Mosbach, "Molecularly imprinted polymers and their use in biomimetic sensors," *Chem. Rev.*, vol. 100, no. 7, pp. 2495–2504, 2000.

[16] J. Bujes-Garrido and M. J. Arcos-Martínez, "Disposable sensor for electrochemical determination of chloride ions," *Talanta*, vol. 155, pp. 153–157, 2016.

[17] S. A. Piletsky, N. W. Turner, and P. Laitenberger, "Molecularly imprinted polymers in clinical diagnostics-Future potential and existing problems," *Med. Eng. Phys.*, vol. 28, no. 10, pp. 971–977, 2006.

[18] D. Nandni, T. S. Lobana, and R. K. Mahajan, "Investigation of chloride ion-sensing property of polymeric membrane and coated graphite sensors based on bis(furan-2-carbaldehyde-N-methylthiosemicarbazonato)nickel(II) complex," *Anal. Lett.*, vol. 42, no. 15, pp. 2474–2484, 2009.

[19] V. A. T. Dam, M. A. G. Zevenbergen, and R. Van Schaijk, "Flexible chloride sensor for sweat analysis," *Procedia Eng.*, vol. 120, pp. 237–240, 2015.

[20] A. T. Piala, T. M. Moon, R. Akella, H. He, M. H. Cobb, and E. J. Goldsmith, "Chloride sensing by WNK1 involves inhibition of autophosphorylation," *Sci. Signal.*, vol. 7, no. 324, pp. 1–10, 2014.

[21] A. Nag, S. C. Mukhopadhyay, and J. Kosel, "Sensing system for salinity testing using laser-induced graphene sensors," *Sensors Actuators, A Phys.*, vol. 264, pp. 107–116, 2017.

[22] F. Pargar, D. A. Koleva, and K. Van Breugel, "Determination of chloride content in cementitious materials: From fundamental aspects to application of Ag/AgCl chloride sensors," *Sensors (Switzerland)*, vol. 17, no. 11, pp. 1–22, 2017.

[23] N. Komal, "Synthesis , Characterization and Physical Properties of Nano-Antimony Oxyhalides," 2017.

[24] M. Tahir, "CO_2 Sorption-Desorption and Physical Properties of $BaCO_3$/CuO Composites ," 2017.

[25] A. A. Bunaciu, E. gabriela Udriştioiu, and H. Y. Aboul-Enein, "X-Ray Diffraction: Instrumentation and Applications," *Crit. Rev. Anal. Chem.*, vol. 45, no. 4, pp. 289–299, 2015.

[26] M. Qammar, " Syntheis Characterization and Antibacterial Activity of Nano-Magnesium Nickel Oxide," 2017.

[27] Kacher, J., Landon, C., Adams, B. L., and Fullwood, " D. Bragg's law diffraction simulations for electron backscatter diffraction analysis, " *Ultramicroscopy*, vol. *109*, no. 9, pp.1148-1156, 2009

[28] L. Lutterotti, "X-ray diffraction : theory and applications to materials science and engineering."

[29] C.O Ruud, and P. C. Chen. " Application of an advanced XRD instrument for surface stress-tensor measurements on steel sheets, " *Experimental Mechanics,* vol.25. no. 3 , pp. 245-250, 1985.

[30] J. K. Patra and K. H. Baek, "Green Nanobiotechnology: Factors Affecting Synthesis and Characterization Techniques," *J. Nanomater.*, vol. 2014, 2014.

[31] O. P. Choudhary and P. ka, "Scanning Electron Microscope: Advantages and Disadvantages in Imaging Components," *Int. J. Curr. Microbiol. Appl. Sci.*, vol. 6, no. 5, pp. 1877–1882, 2017.

[32] B. Driskill, J. Walls, J. DeVito, S. W. Sinclair, "11 Applications of SEM Imaging to Reservoir Characterization in the Eagle Ford Shale, South Texas, USA," pp.115-136, 2013.

[33] M.Leka, J.W. Zuber, "Biomedical applications of AFM, "*Journal of Physics: Conference Series*. Vol. 146.no. 1, 2009 .

[34] H. Thorsten S. Markus "The study of molecular interactions by AFM force spectroscopy, "*Macromolecular rapid communications*, vol.*22*, no.13, pp.989-1016 ,2001.

[35] C. Yu, L. Zhang, J. Shi, J. Zhao, J. Gao, and D. Yan, "A simple template-free strategy to synthesize nanoporous manganese and nickel oxides with narrow pore size distribution, and their electrochemical properties," *Adv. Funct. Mater.*, vol. 18, no. 10, pp. 1544–1554, 2008.

[36] Y. Wenbo, "Mesoporous Crystalline Metal Oxides," 2009.

[37] A. Ivanova, "Nanoporous Metal Oxides Templated by Nanocrystalline Cellulose," 2015.

[38] "Standard Test Method for Advanced Ceramic Specific Surface Area by Physical," pp. 1–9, 2012.

[39] "Pore size distribution and porosity of solid materials by mercury porosimetry and gas adsorption ," 2010.

[40] J.C.Y David, "Physical and Chemical Adsorption measurment of solid surface areas " .

[41] S. Kenneth,"The use of nitrogen adsorption for the characterisation of porous materials, , *Colloids and Surfaces A: Physicochemical and Engineering Aspects*, vol.*187*, pp.3-9, 2001.

[42] J.C.P.Broekhoff, J.H.De Boer ,"Studies on pore systems in catalysts: X. Calculations of pore distributions from the adsorption branch of nitrogen sorption isotherms in the case of open cylindrical pores B. Applications, "*Journal of Catalysis* , vol.9, no.1, pp.15-27 ,1967.

[43] .Choi, C, "An Introductory Laboratory Course for Electrical Engineering Majors."

[44] M.A.AtmanandV, K.Jagadeesh, "Microcontroller based LCR meter",vol 20, no.5 pp. 297-301, 1996

[45] J. Desroches, P. A. Champagne, Y. Benhassine, J.-F. Paquin, M. Lukacs, and D. Bhadra, *Org. Biomol. Chem.*, vol. 13, no. 8, pp. 2243–2246, 2015.

[46] M. Vakilian and B. Y. Majlis, "Study of interdigitated electrode sensor for lab-on-chip applications," *IEEE Int. Conf. Semicond. Electron. Proceedings, ICSE*, pp. 201–204, 2014.

[47] S. Z. Bajwa, R. Dumler, and P. A. Lieberzeit, "Molecularly imprinted polymers for conductance sensing of $Cu2+$in aqueous solutions," *Sensors Actuators, B Chem.*, vol. 192, pp. 522–528, 2014.

[48] W. H. Grover, "Interdigitated Array Electrode Sensors : Their Design , Efficiency , and Applications," *Honor. thesis , Univ. Tennessee*, vol. 3, pp. 1–62, 1999.

[49] B. D. Zdravkov, J. J. Čermák, M. Šefara, and J. Janků, "Pore classification in the characterization of porous materials: A perspective," *Cent. Eur. J. Chem.*, vol. 5, no. 2, pp. 385–395, 2007.

[50] C. J. Brinker, "Porous inorganic materials," pp. 798–805, 1994.

[51] B. G. Trewyn, I. I. Slowing, H. Chen, and V. S. Lin, "Synthesis and Functionalization of a Mesoporous Silica Nanoparticle Based on the Sol − Gel Process and Applications in Controlled Release Synthesis and Functionalization of a Mesoporous Silica Nanoparticle Based on the Sol − Gel Process and Applications i," pp. 846–853, 2007.

[52] C. Chartier, S. Bastide, and C. Levy-Clement, "Metal-assisted chemical etching of silicon in $HF–H_2O_2$" *Electrochim. Acta*, vol. 53, no. 17, pp. 5509–5516, 2008.

[53] N. I. Vazquez, Z. Gonzalez, B. Ferrari, and Y. Castro, "Synthesis of mesoporous silica nanoparticles by sol-gel as nanocontainer for future drug delivery applications," *Bol. la Soc. Esp. Ceram. y Vidr.*, vol. 56, no. 3, pp. 139–145, 2017.

[54] Ubat, Penyebaran, "Microwave-assisted synthesis of mesoporous silica nanoparticles as a drug delivery vehicle ," *Malaysian J. Anal. Sci.*, vol. 20, no. 6, pp. 1382–1389, 2016.

[55] E. B. Celer and M. Jaroniec, "Temperature-programmed microwave-assisted synthesis of SBA-15 ordered mesoporous silica," *J. Am. Chem. Soc.*, vol. 128, no. 44, pp. 14408–14414, 2006.

[56] S. Kumar, M. M. Malik, and R. Purohit, "Synthesis Methods of Mesoporous Silica Materials," *Mater. Today Proc.*, vol. 4, no. 2, pp. 350–357, 2017.

[57] S.-H. Wu, C.-Y. Mou, and H.-P. Lin, "Synthesis of mesoporous silica nanoparticles," *Chem. Soc. Rev.*, vol. 42, no. 9, p. 3862, 2013.

[58] W.Gunter, "Molecular Imprinting in Cross-Linked Materials with the Aid of Molecular Templates. A Way towards Artificial Antibodies," *Angewandte Chemie International Edition in English.*,vol.17, no.17,pp.1812-1832, 1995.

[59] W. Bingbing, J.Ping, J. Shidong, L. Yamai, ".Synthesis of NaCl Single Crystals with Defined Morphologies as Templates for Fabricating Hollow Nano/micro-structures." *Royal Society Of Chemistry*.

[60] Wang, Bingbing, Ping Jin, Yuanzheng Yue, Shidong Ji, Yamei Li, and Hongjie Luo , "Synthesis of NaCl single crystals with defined morphologies as templates for fabricating hollow nano/micro-structures," *Rsc Advances,* vol. 5, no. 7, pp. 5072-5076, 2015.

[61] R. Liu, S. Yang, F. Wang, X. Lu, Z. Yang, and B. Ding, "Sodium chloride template synthesis of cubic tin dioxide hollow particles for lithium ion battery applications," *ACS Appl. Mater. Interfaces*, vol. 4, no. 3, pp. 1537–1542, 2012.

[62] B. Klewe and B. Pedersen, "The crystal structure of sodium chloride dihydrate," *Acta Crystallogr. Sect. B Struct. Crystallogr. Cryst. Chem.*, vol. 30, no. 10, pp. 2363–2371, 1974.

[63] Z.Weiwei, R.O Artem, F. G. Alexander, Z. Qiang, E. B Salah. O .L Andriy, S.Elissaios, S. Maddury, B. P Vitali, K. Zuzana, "Unexpected stable stoichiometries of sodium chlorides," *Science (80-.).*, vol. 342, no. 6165, pp. 1502–1505, 2013.

[64] L. C. Sow and H. Yang, "Effects of salt and sugar addition on the physicochemical properties and nanostructure of fish gelatin," *Food Hydrocoll.*, vol. 45, pp. 72–82, 2015.

[65] A. Mujahid, P. A. Lieberzeit, and F. L. Dickert, "Chemical sensors based on molecularly imprinted sol-gel materials," *Materials (Basel).*, vol. 3, no. 4, pp. 2196–2217, 2010.

[66] G.F Marcos, A.R Jose, "Metal Oxide Nanoparticles," *Encycl. Inorg. Chem.*, no. October, 2009.

[67] Z. Sun, "Strategies for designing metal oxide nanostructures Strategies for designing metal oxide nanostructures," vol. 60, no. January, pp. 1–24, 2017.

[68] R. Newman and R. M. Chrenko, "Optical Properties of Nickel Oxide," *Phys. Rev.*, vol. 114, no. 6, pp. 1507–1513, 1959.

[69] R. R. Dessai, J. A. E. Desa, D. Sen, and P. D. Babu, "Nanometric study of Nickel Oxide Prepared by Sol Gel Process," vol. 050052, 2018.

[70] A. Cimino, M. Lo Jacono, and M. Schiavello, "Structural, magnetic, and optical properties of nickel oxide supported on .eta.- and .gamma.-aluminas," *J. Phys. Chem.*, vol. 75, no. 8, pp. 1044–1050, 1971.

[71] Dhaouadi, Mehdi, Mohamed Jlassi, Imen Sta, Islem Ben Miled, George Mousdis, Michael Kompitsas, and Wissem Dimassi., "Physical Properties of Copper Oxide Thin Films Prepared by Sol – Gel Spin – Coating Method," *Am. J. Phys. Appl.*, vol. 6, no. 2, pp. 43–50, 2018.

[72] D. Gupta, S. R. Meher, N. Illyaskutty, and Z. C. Alex, "Facile synthesis of Cu2O and CuO nanoparticles and study of their structural, optical and electronic properties," *J. Alloys Compd.*, vol. 743, pp. 737–745, 2018.

[73] Z. Qiaobao, Z. Kaili , X. Daguo,Y. Guangcheng, H. Hui, N. Fude, L.Chenmin, Y.Shihe, "CuO nanostructures: Synthesis, characterization, growth mechanisms, fundamental properties, and applications," *Prog. Mater. Sci.*, vol. 60, no. 1, pp. 208–237, 2014.

[74] R. Madhu, V. Veeramani, S. M. Chen, A. Manikandan, A. Y. Lo, and Y. L. Chueh, "Honeycomb-like Porous Carbon-Cobalt Oxide Nanocomposite for High-Performance Enzymeless Glucose Sensor and Supercapacitor Applications," *ACS Appl. Mater. Interfaces*, vol. 7, no. 29, pp. 15812–15820, 2015.

[75] Mock, Alyssa, K. Rafal , B. Chad, S. Derek, H. Tino, W. Peter, S. Alexander , S.Eva, S.Mathias,"Anisotropy, band-to-band transitions, phonon modes, and oxidation properties of cobalt-oxide core-shell slanted columnar thin films," *Appl. Phys. Lett.*, vol. 108, no. 5, 2016.

[76] J. Park, X. Shen, and G. Wang, "Solvothermal synthesis and gas-sensing performance of Co3O4hollow nanospheres," *Sensors Actuators, B Chem.*, vol. 136, no. 2, pp. 494–498, 2009.

[77] D. Shi, M. E. Sadat, A. W. Dunn, and D. B. Mast, "Photo-fluorescent and magnetic properties of iron oxide nanoparticles for biomedical applications," *Nanoscale*, vol. 7, no. 18, pp. 8209–8232, 2015.

[78] Y. Bustami, M. Moo-Young, and W. A. Anderson, "Analysis of the heterogeneous structure of iron oxide/gold nanoparticles and their application in a nanosensor," *Sensors Actuators, B Chem.*, vol. 245, pp. 753–764, 2017.

[79] M. Iv, N. Telischak, D. Feng, S. . Holdsworth, K. . Yeom, and H. . Daldrup-Link, "Clinical applications of iron oxide nanoparticles for magnetic resonance imaging of brain tumors," *Nanomedicine (Lond).*, vol. 10, no. 6, pp. 993–1018, 2015.

[80] S.C.Chopade, I.G.Kore, S.P.Pati ,ln .D.Jadhav, C.Srinidhi, P.A.Desai, "Lattice geometry controlled synthesis of Cu − Doped nickel oxide nanoparticles, " *Ceramics International*, vol.44, pp.5621-5628, 2018.

[81] B. Keimer, S. A. Kivelson, M. R. Norman, S. Uchida & J. Zaanen, "From quantum matter to high-temperature superconductivity in copper oxides," *Nature.*,vol.518 ,pp.179-186, 2015.

[82] JS Olsen, CSG Cousins, L Gerward, H Jhans, " J. A A study of the crystal structure of Fe_2O_3 in the pressure range up to 65 GPa using synchrotron radiationm".*Physica Scripta*.,vol.43, no.3, pp.13925-13931,1991.

[83] M.Y.Tian, D shang, "Metal–Organic Framework Derived Hybrid Co_3O_4-Carbon Porous Nanowire Arrays as Reversible Oxygen Evolution Electrodes" *J. Am. Chem. Soc*.,vol.136, no.39, pp.13925-13931, 2014.

[84] M. M. Titirici, M. Antonietti, and A. Thomas, "A generalized synthesis of metal oxide hollow spheres using a hydrothermal approach," *Chem. Mater.*, vol. 18, no. 16, pp. 3808–3812, 2006.

[85] X. Sun, J. Liu, and Y. Li, "Use of carbonaceous polysaccharide microspheres as templates for fabricating metal oxide hollow spheres," *Chem. - A Eur. J.*, vol. 12, no. 7, pp. 2039–2047, 2006.

[86] M. Sadakane, T. Horiuchi, N. Kato, C. Takahashi, and W. Ueda, "Facile preparation of three-dimensionally ordered macroporous alumina, iron oxide, chromium oxide, manganese oxide, and their mixed-metal oxides with high porosity," *Chem. Mater.*, vol. 19, no. 23, pp. 5779–5785, 2007.

[87] J. S. Hu, L. S. Zhong, W. G. Song, and L. J. Wan, "Synthesis of hierarchically structured metal oxides and their application in heavy metal ion removal," *Adv. Mater.*, vol. 20, no. 15, pp. 2977–2982, 2008.

[88] S. M. L. Dos Santos, K. A. B. Nogueira, M. De Souza Gama, J. D. F. Lima, I. J. Da Silva Júnior, and D. C. S. De Azevedo, "Synthesis and characterization of ordered mesoporous silica (SBA-15 and SBA-16) for adsorption of biomolecules," *Microporous Mesoporous Mater.*, vol. 180, pp. 284–292, 2013.

[89] X. Deng, K. Chen, and H. Tüysüz, "Protocol for the Nanocasting Method: Preparation of Ordered Mesoporous Metal Oxides," *Chem. Mater.*, vol. 29, no. 1, pp. 40–52, 2017.

[90] P. Swasmi, Z. Hongwei, H. Xiaodan, S. Hao, Y. Yannan, Z. Jun, N. Yuting, M.K. Anand, N. Owen, and Y.Chengzhong., "Mesoporous Magnesium Oxide Hollow Spheres as Superior Arsenite Adsorbent: Synthesis and Adsorption Behavior," *ACS Appl. Mater. Interfaces*, vol. 8, no. 38, pp. 25306–25312, 2016.

[91] X. Xu, S. Huaibing, L.shizhi, Z.Ying, H.Zhimi, S.Jiyo, Y.Bo, L.Tianqi, Z. Jun, T.Jiang ., "Scalable salt-templated synthesis of two-dimensional transition metal oxides," *Nat. Commun.*, vol. 7, pp. 1–8, 2016.

[92] S. Rahmani, D.Jean Olivier, C. Clarence., "Synthesis of mesoporous silica nanoparticles and nanorods: Application to doxorubicin delivery," *Solid State Sci.*, vol. 68, pp. 25–31, 2017.

[93] B. V Romanovsky, A. A. Maerle, A. A. Karakulina, and I. F. Moskovskaya, "Ultrasound-Assisted Synthesis of Nanostructured Transition Metal Oxides," vol. 72, no. 1, pp. 42–48, 2017.

[94] A. S. Golezani, A. S. Fateh, and H. A. Mehrabi, "Synthesis and characterization of silica mesoporous material produced by hydrothermal continues pH adjusting path way," *Prog. Nat. Sci. Mater. Int.*, vol. 26, no. 4, pp. 411–414, 2016.

[95] L. Wenge, H. Yanjie , J.Hao, J. Yi, W. Yang, H. Su, B. Pratim, L. Chunzhong ., "Fluxing template-assisted synthesis of sponge-like Fe_2O_3 microspheres toward efficient catalysis for CO oxidation, " vol. 444. 2018.

[96] P. P. Wang, Y. X. Zhang, X. Y. Fan, J. X. Zhong, and K. Huang, "Synthesis of Si nanosheets by using Sodium Chloride as template for high-performance lithium-ion battery anode material," *J. Power Sources*, vol. 379, no. January, pp. 20–25, 2018.